RESEARCH ARTICLE

Check for updates

Design, synthesis and biological evaluation of *N*-pyridinyl ureidobenzenesulfonates and their hydrochloride salts as novel water-soluble dihydroorotate dehydrogenase inhibitors inducing differentiation of acute myeloid leukemia cells†

Vincent Ouellette, [iD] ‡[ab] Chahrazed Bouzriba,‡[ab] Atziri Corin Chavez Alvarez,[abc] Geneviève Hamel-Côté[a] and Sébastien Fortin [iD] *[ab]

A series of novel dihydroorotate dehydrogenase (DHODH) inhibitors designated as *N*-pyridinyl ureidobenzenesulfonates (PYRUB-SOs) and their hydrochloride salts were designed, synthesized, and evaluated for their biological activity. PYRUB-SOs exhibit antiproliferative activity at submicromolar to low micromolar concentrations on various cancer cell lines, including notably acute myeloid leukemia (AML) MOLM-13, THP-1 and HL-60 cells. Moreover, PYRUB-SO salts display higher aqueous solubility (up to 10 times) compared to their neutral counterparts. Additionally, the most potent PYRUB-SOs and their salts effectively arrest the progression of the cell cycle in the S-phase and induce the phosphorylation of histone H2AX, an indicator of replicative stress. They also inhibit DHDOH activity (IC_{50} = 12–31 nM). In addition, molecular docking studies show their stable binding modes in the brequinar-binding site of DHODH. Furthermore, PYRUB-SOs trigger the differentiation of a significant portion of the population of both MOLM-13 and THP-1 cells, as evidenced by increased CD11b single expression and increased CD11b and CD14 dual expression, respectively. Finally, they exhibit metabolic stability with half-lives varying from 57 to 216 min in rodent and human liver microsomes. Our study highlights that the new PYRUB-SO salts improve the water solubility of this new family of DHODH inhibitors while maintaining their biological activity.

1 Introduction

Cancer is a major health hazard affecting nearly 20 million people and was responsible for approximately 9.7 million deaths worldwide in 2022.[1] Despite advances in diagnosis and treatments, cancer remains one of the leading causes of death worldwide. Consequently, the research and the development of new molecules and anticancer therapies are still indispensable, especially against cancer exhibiting poor

[a] Centre de recherche du CHU de Québec-Université Laval, Axe Oncologie, Hôpital Saint-François d'Assise, 10 rue de l'Espinay, Québec, QC, G1L 3L5, Canada. E-mail: vincent.ouellette.2@ulaval.ca, chahrazed.bouzriba.1@ulaval.ca, atziri-corin.chavez-alvarez.1@ulaval.ca, genevieve.hamel-cote@crchudequebec.ulaval.ca, sebastien.fortin@pha.ulaval.ca; Tel: +1 (418) 525 4444 ext. 52364
[b] Faculté de pharmacie, Université Laval, 1050 avenue de la Médecine, Québec, QC, G1V 0A6, Canada
[c] Centre de recherche de l'Institut universitaire de cardiologie et de pneumologie de Québec-Université Laval, 2725 Ch Ste-Foy, Québec, QC, G1V 4G5, Canada
† Electronic supplementary information (ESI) available. See DOI: https://doi.org/10.1039/d5md00171d
‡ These authors contributed equally to this work.

prognosis such as acute myeloid leukemia (AML).[2] AML is a heterogeneous and aggressive hematological cancer that primarily affects adults above 65 years old, although it can occur at any age.[3] The prognosis for AML remains poor, with a 5-year overall survival rate for adults of 31.9%.[4] AML is characterized by the blockage of myeloid cell differentiation, resulting in the rapid proliferation of immature myeloid cells. The accumulation of these immature precursor cells in the bone marrow and blood disrupts the normal functioning of hematopoiesis, leading to anaemia, infections and hemorrhages.[5] The standard chemotherapeutic treatment for AML remains, after more than 40 years, a combination of cytarabine and daunorubicin, which is poorly tolerated, often ineffective, and leading to high rates of resistance and relapse.[6]

Recent findings in the molecular characterization of AML identified numerous genetic and epigenetic mutations that drive the disease and are the cornerstones that will lead to the development of new targeted therapies.[7] For example, inhibitors targeting specific mutations, such as FLT3 and IDH1/2 inhibitors have shown promise in clinical trials and are now approved for use in certain patient subsets.[8]

However, the genetic complexity and the clonal heterogeneity of AML require the development of novel and broader-acting drugs to improve both the life expectancy and the quality-of-life of patients with all AML subtypes. In that perspective, a promising approach currently under investigation is the AML cell differentiation therapy using dihydroorotate dehydrogenase (DHODH) inhibitors.[9–12]

DHODH is an essential mitochondrial enzyme involved in the fourth step of *de novo* synthesis of pyrimidines. This enzyme catalyzes the conversion of dihydroorotate to orotate, which is a key step in the production of uridine monophosphate (UMP), a nucleotide required for DNA and RNA synthesis.[13] Due to its pivotal role in nucleotide biosynthesis, DHODH has emerged as a potential therapeutic target in various proliferative pathologies such as AML, targeting metabolic pathways essential for leukemic cell survival and proliferation.[14] Indeed, the conversion of dihydroorotate to orotate *via* the *de novo* synthesis pathway is crucial in cancer cells to sustain their proliferation.[15] Several DHODH inhibitors have been developed[16–19] and clinically studied over the years, such as Arava (leflunomide, Fig. 1A),[20] farudodstat (ASLAN003, Fig. 1B)[21] and brequinar (DUP-785, Fig. 1C),[22] which are underlying the importance of developing those inhibitors.

Our research group has been developing novel DHODH inhibitors based on a pharmacophoric entity named *N*-phenyl ureidobenzenesulfonates (PUB-SOs, Fig. 1D).[23–26] Our recent studies highlighted that PUB-SOs exhibit antiproliferative activity in the submicromolar to micromolar concentration range on several cancer cell lines, including HT-1080 (human fibrosarcoma), MCF7 (breast adenocarcinoma), HT-29 (colon adenocarcinoma) and M21

(skin melanoma) cells. They also arrest the cell cycle progression in the S-phase and induce histone H2AX phosphorylation, an indicator of replicative stress. Moreover, our research program identified several PUB-SOs such as SFOM-0046 (Fig. 1E) as potent DHODH inhibitors with IC_{50} within the nanomolar range. Furthermore, they are more potent against leukemic cells, and they induce both apoptosis and differentiation of AML cells into CD11b and CD14 positive cells.[27]

However, despite their promising properties, PUB-SOs suffer from an important drawback: they are sparingly water-soluble, limiting their doses administered for *in vivo* experiments. This constraint might be an impediment to their preclinical development. To overcome this problem, an ionizable function was incorporated into the molecular structure of PUB-SOs to form their corresponding hydrochloride salts. This involved the substitution of the aromatic ring B of PUB-SOs by a pyridinyl ring, resulting in the development of innovative *N*-pyridinyl ureidobenzenesulfonates (PYRUB-SOs) along with their hydrochloride salts. Therefore, this study details their design, synthesis, water solubility evaluation, and their mechanism of action through various biofunctional assays. First, PYRUB-SOs and their hydrochlorides were assessed for their water solubility and antiproliferative activity on several cancer cell lines, including AML cells. Then, prototypical PYRUB-SOs and their hydrochloride salts were selected to determine their hydrosolubility before *in vitro* testing. Thereafter, the most potent PYRUB-SOs and their hydrochlorides were evaluated for their antiproliferative activity on several cancer cell lines, including AML, their impact on the cell cycle progression, and their potential to induce H2AX phosphorylation. In
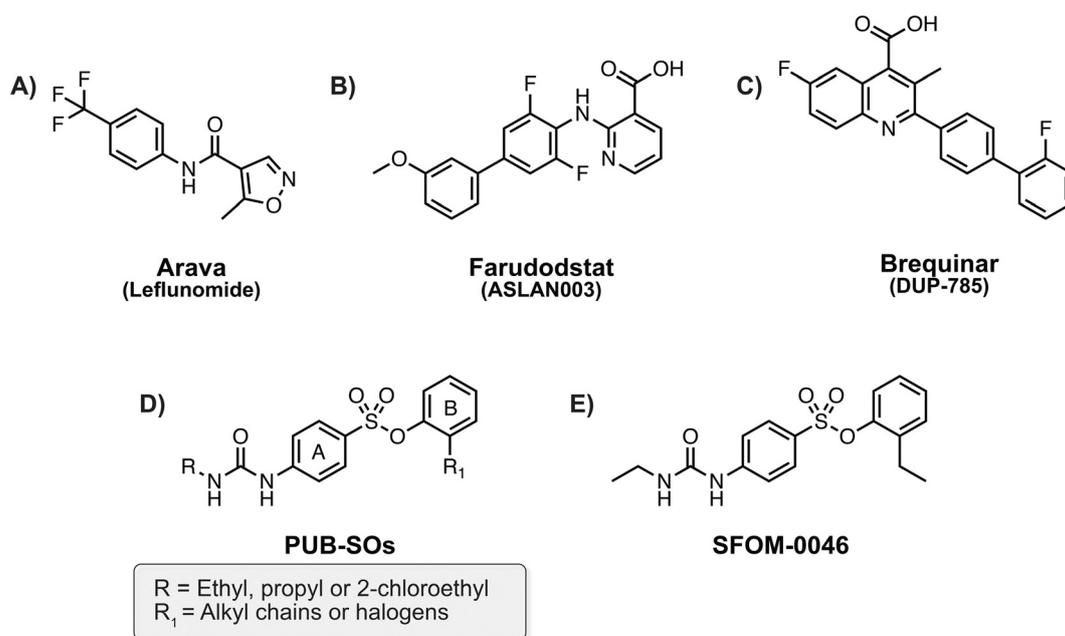
Fig. 1 Molecular structures of A) Arava (leflunomide), B) farudodstat (ASLAN003), C) brequinar (DUP-785), D) *N*-phenyl ureidobenzenesulfonates (PUB-SOs) and E) SFOM-0046.

addition, their effects on DHODH activity and the differentiation of selected AML cell lines were assessed. Finally, the druglikeness properties and the metabolic stability of PYRUB-SOs were evaluated using *in silico* predictive models SwissADME[28] as well as rodent and human liver microsomes, respectively.

## 2 Results and discussion

2.1 Design and chemistry

The substituted pyridinyl group was incorporated into the molecular structure of PUB-SOs because their nitrogen atom acts as a weak base (pK_a ≈ 4–5) and that they can generate salt compounds when interacting with strong inorganic acids such as hydrochloric acid (pK_a ≈ −6).[29–31] Indeed, the pyridinyl scaffold is a rational choice because of its wide use in drug development to modify the physicochemical properties of novel drugs and generate water-soluble salts.[32–37] Our previous structure–activity relationship (SAR) studies on PUB-SOs evidenced that the aromatic ring A is highly sensitive to structural modifications. Therefore, a pyridinyl group was substituted on aromatic ring B. Furthermore, the nitrogen atom was strategically introduced at positions 3 or 5 of the pyridinyl ring to evaluate the influence of its position on the overall antiproliferative activity. Our previous SAR studies on PUB-SOs also underlined the importance of incorporating either an ethyl, propyl, or 2-chloroethyl group on the urea moiety along with either halogen atoms or bulky alkyl groups at position 2 on the phenyl ring B to achieve significant antiproliferative activity on cancer cells.[23–25] Consequently, we aimed to

synthesize novel PYRUB-SOs with these substitution characteristics. We also selected the formation of hydrochloride salts because they are abundant in marketed drugs and that their low pK_a promotes the formation of the hydrochloride salt in the presence of a pyridinyl group.[37,38]

The preparation of PYRUB-SOs **1–18** and their hydrochlorides **19–36** is illustrated in Scheme 1. The synthesis was achieved in 3 steps for the neutral compounds and in 4 steps for their corresponding hydrochlorides from the selected aniline. First, the synthesis of starting precursors **37–39** and **40–42** was adapted from Gagné-Boulet *et al.* Of note, compounds **39** and **42** were previously reported by Gagné-Boulet *et al.*[24] Briefly, the synthesis of the phenylureas **37–39** began with the electrophilic addition of the relevant isocyanate to aniline in diethyl ether. Afterwards, chlorosulfonation of **37–39** with chlorosulfonic acid afforded sulfonyl chlorides **40–42**. Then, the desired PYRUB-SOs **1–18** were prepared by reacting sulfonyl chlorides **40–42** with the appropriate pyridinol in the presence of triethylamine in methylene chloride with yields ranging from 13 to 75%. Finally, the PYRUB-SO hydrochloride salts **19–36** were prepared by reacting hydrogen chloride solution (in diethyl ether) with PYRUB-SOs **1–18** in THF with yields ranging from 73 to 98%.

2.2 Water solubility evaluation

One of the primary goals of substituting the phenyl ring B of PUB-SOs with a bioisosteric pyridinyl group was to enhance water solubility by forming hydrochloride salts. This modification aimed to increase their concentration in
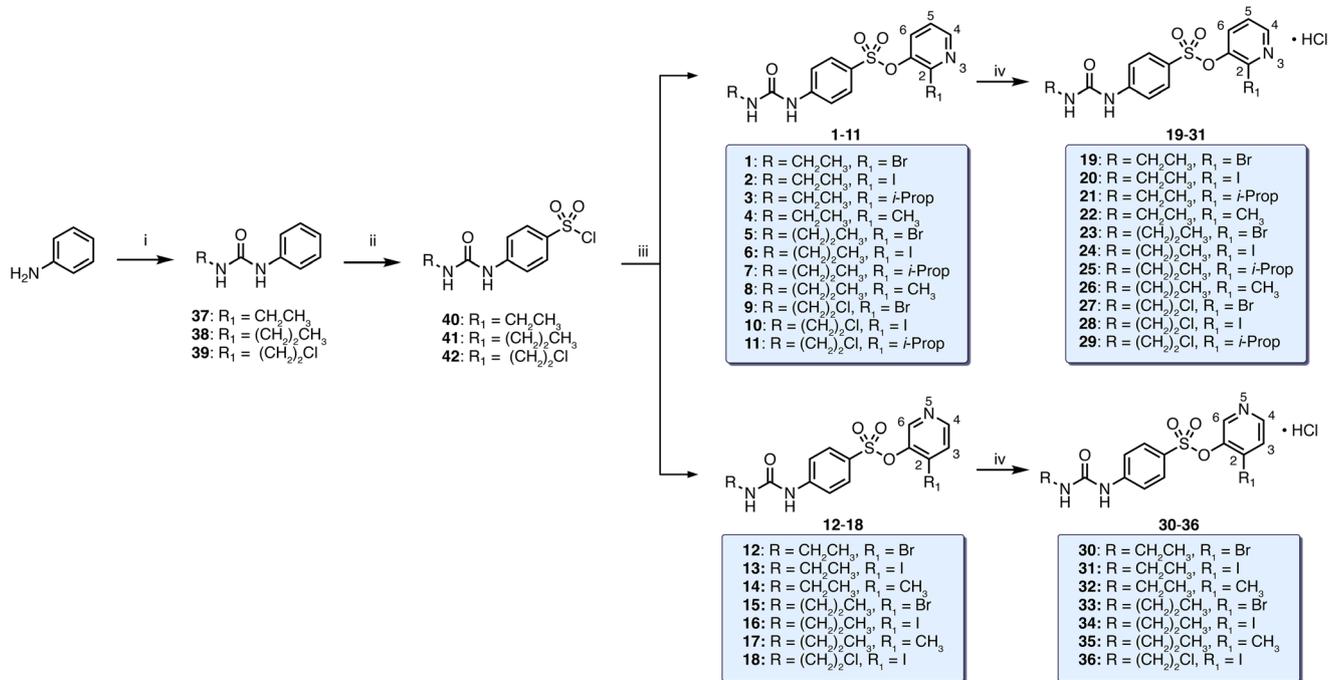
Scheme 1 General synthesis of PYRUB-SOs **1–36**. Reagents and conditions: (i) relevant isocyanate, Et$_2$O, 0 °C to rt, 16 h; (ii) ClSO$_3$H, 0 °C to 60 °C, 1 h; (iii) relevant pyridinol, TEA/DCM, rt, 48 h; (iv) HCl/Et$_2$O, THF, rt, 16 h.

RSC Medicinal Chemistry

the excipients used to conduct the biofunctional assays and, ultimately, in the pharmaceutical formulations prepared for further *in vivo* studies. Consequently, the water solubility of PYRUB-SOs **1–18** and their hydrochlorides **19–36** were assessed using UV spectroscopy and the results are collated in Table 1. PUB-SO homologs SFOM-0106, SFOM-0107, SFOM-0111, SFOM-0147, SFOM-0148, and SFOM-0149, respectively, bearing an iodine atom or an isopropyl group were selected for the sake of comparison. Our results show that all studied PUB-SO homologs studied so far are sparingly soluble in water, with water solubilities ranging from 4.5 to 18 $\mu g\ mL^{-1}$. The water solubility of neutral PYRUB-SOs **1–18** ranges from 4.4 to 64 $\mu g\ mL^{-1}$, while the water solubility of their hydrochlorides **19–36** ranges from 26 to 190 $\mu g\ mL^{-1}$. These results indicate that replacing the phenyl ring B of PUB-SOs with a pyridinyl ring and forming their corresponding hydrochlorides generally enhance their water solubility by factors up to 9- and 42-fold, respectively, compared with their studied PUB-SO counterparts. Moreover, the results evidenced that the formation of hydrochlorides increases the water solubility of PYRUB-SOs counterparts by factors ranging between 2- to 10-fold. In summary, our results show that PYRUB-SOs and their hydrochlorides are more water-soluble than their PUB-SO
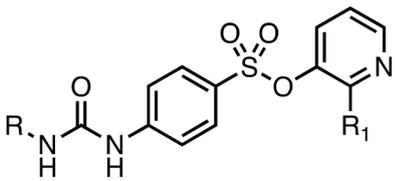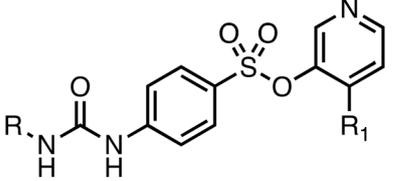
counterparts, suggesting that both the substitution of the phenyl ring with a pyridinyl group and the formation of hydrochloride salt are promising strategies to improve the water solubility of PUB-SOs.

2.3 Biological evaluation

2.3.1 Antiproliferative activity of PYRUB-SOs on non-AML human cancer cell lines. We first assessed the antiproliferative activity of PYRUB-SOs **1–18** and their hydrochloride salts **19–36** on a panel of 4 adherent non-AML human tumour cell lines named MCF7 (breast adenocarcinoma), M21 (melanoma), HT-29 (colorectal adenocarcinoma) and HT-1080 (fibrosarcoma), respectively. The half-maximal inhibitory concentration (IC_{50}) for each compound was determined using the procedure detailed by the NIH NCI-60 human tumour cell lines screening protocol with minor modifications.[39] SFOM-0046 and brequinar were used as reference and positive controls. The results are reported in Table 2. Our results show that the IC_{50} of PYRUB-SOs and their corresponding hydrochlorides are usually in the same order of magnitude as those of PUB-SOs.[23–25] This suggests that the substitution of the phenyl ring B of PUB-SOs with a pyridinyl group and the formation of

Table 1 Water solubility of PYRUB-SOs **1–18**, their hydrochloride salts **19–36** and their PUB-SO counterparts (SFOM-0106, SFOM-0107, SFOM-0111, SFOM-0147, SFOM-0148 and SFOM-0149)[23–25]

1-11 and **19-29** (hydrochlorides) | **12-18** and **30-36** (hydrochlorides)

#	R	R1	Solubility[a] ($\mu g\ mL^{-1}$)	#	R	R1	Solubility[a] ($\mu g\ mL^{-1}$)
1	CH_2CH_3	Br	64 ± 1	22	CH_2CH_3	CH_3	152 ± 4
2	CH_2CH_3	I	57 ± 3	23	$(CH_2)_2CH_3$	Br	79 ± 9
3	CH_2CH_3	i-Prop	40 ± 3	24	$(CH_2)_2CH_3$	I	120 ± 10
4	CH_2CH_3	CH_3	55 ± 1	25	$(CH_2)_2CH_3$	i-Prop	26 ± 3
5	$(CH_2)_2CH_3$	Br	8 ± 1	26	$(CH_2)_2CH_3$	CH_3	151 ± 1
6	$(CH_2)_2CH_3$	I	23 ± 2	27	$(CH_2)_2Cl$	Br	189 ± 5
7	$(CH_2)_2CH_3$	i-Prop	7 ± 1	28	$(CH_2)_2Cl$	I	37 ± 2
8	$(CH_2)_2CH_3$	CH_3	44 ± 1	29	$(CH_2)_2Cl$	i-Prop	126 ± 5
9	$(CH_2)_2Cl$	Br	56 ± 2	30	CH_2CH_3	Br	122 ± 4
10	$(CH_2)_2Cl$	I	4.4 ± 0.1	31	CH_2CH_3	I	165 ± 3
11	$(CH_2)_2Cl$	i-Prop	41 ± 3	32	CH_2CH_3	CH_3	98 ± 7
12	CH_2CH_3	Br	64 ± 1	33	$(CH_2)_2CH_3$	Br	124 ± 2
13	CH_2CH_3	I	63 ± 1	34	$(CH_2)_2CH_3$	I	130 ± 10
14	CH_2CH_3	CH_3	49 ± 4	35	$(CH_2)_2CH_3$	CH_3	138 ± 2
15	$(CH_2)_2CH_3$	Br	35 ± 3	36	$(CH_2)_2Cl$	I	154 ± 7
16	$(CH_2)_2CH_3$	I	53 ± 6	SFOM-0149	CH_2CH_3	I	8 ± 2
17	$(CH_2)_2CH_3$	CH_3	52 ± 2	SFOM-0111	CH_2CH_3	i-Prop	4.5 ± 0.5
18	$(CH_2)_2Cl$	I	24 ± 2	SFOM-0148	$(CH_2)_2CH_3$	I	14 ± 1
19	CH_2CH_3	Br	173 ± 2	SFOM-0147	$(CH_2)_2CH_3$	i-Prop	13 ± 1
20	CH_2CH_3	I	190 ± 10	SFOM-0106	$(CH_2)_2Cl$	I	18 ± 1
21	CH_2CH_3	i-Prop	188 ± 1	SFOM-0107	$(CH_2)_2Cl$	i-Prop	15 ± 3

[a] Expressed as the mean ± the standard error of the mean (SEM).

Table 2 Antiproliferative activity (IC_{50}) of PYRUB-SOs **1–18**, their hydrochloride salts **19–36**, SFOM-0046 and brequinar on non-AML MCF7, M21, HT-29 and HT-1080 cell lines

Compound	$IC_{50}{}^{a}$ (µM) ± SEM^{b}			
	MCF7	M21	HT-29	HT-1080
1	31 ± 3	12 ± 1	9.7 ± 0.7	2.1 ± 0.3
2	11 ± 1	13 ± 2	10.6 ± 0.9	1.4 ± 0.1
3	19 ± 2	7 ± 1	8.4 ± 0.7	1.2 ± 0.2
4	20 ± 3	79 ± 4	56 ± 3	10.2 ± 0.8
5	13 ± 1	24 ± 2	17 ± 1	3.3 ± 0.2
6	13 ± 1	17 ± 1	16 ± 1	2.0 ± 0.2
7	17 ± 1	22 ± 2	14 ± 1	2.3 ± 0.1
8	19 ± 2	69 ± 3	70 ± 8	5.1 ± 0.5
9	16 ± 1	23 ± 1	17 ± 1	3.8 ± 0.3
10	5 ± 1	9 ± 1	9 ± 1	1.8 ± 0.1
11	17 ± 1	20 ± 1	14 ± 1	3.8 ± 0.2
12	32 ± 4	21 ± 1	25 ± 1	4.1 ± 0.3
13	15 ± 2	9 ± 1	12 ± 1	3.2 ± 0.3
14	31 ± 3	31 ± 3	16 ± 1	9.4 ± 0.7
15	12 ± 1	28 ± 2	19 ± 1	4.1 ± 0.3
16	5 ± 1	9.7 ± 0.9	6.9 ± 0.5	3.1 ± 0.3
17	12 ± 1	24 ± 1	12 ± 1	7.5 ± 0.5
18	2.8 ± 0.4	2.8 ± 0.3	2.7 ± 0.2	1.2 ± 0.1
19	28 ± 2	27 ± 2	26 ± 2	3.3 ± 0.3
20	12 ± 1	7.7 ± 0.7	6.8 ± 0.6	1.1 ± 0.2
21	24 ± 3	11 ± 1	8.0 ± 0.3	1.0 ± 0.2
22	51 ± 5	>100	>100	26 ± 2
23	22 ± 2	45 ± 2	42 ± 2	6.0 ± 0.5
24	22 ± 2	29 ± 2	28 ± 2	4.0 ± 0.3
25	16 ± 1	20 ± 1	15 ± 0.8	2.4 ± 0.2
26	33 ± 4	>100	>100	15 ± 2
27	16 ± 1	30 ± 2	33 ± 1	5.5 ± 0.4
28	13 ± 1	15 ± 1	21 ± 1	3.1 ± 0.2
29	14 ± 1	9.7 ± 0.5	10.5 ± 0.5	3.3 ± 0.2
30	45 ± 4	44 ± 3	45 ± 4	6.7 ± 0.4
31	19 ± 3	11 ± 1	11 ± 1	5.3 ± 0.4
32	26 ± 2	35 ± 4	9.6 ± 0.7	5.9 ± 0.7
33	24 ± 2	40 ± 1	30 ± 1	10.0 ± 0.8
34	13 ± 1	21 ± 2	14 ± 1	5.9 ± 0.5
35	58 ± 8	56 ± 3	39 ± 2	21 ± 2
36	3.8 ± 0.3	3.5 ± 0.4	2.3 ± 0.1	1.2 ± 0.2
SFOM-0046	4.7 ± 0.7	5.3 ± 0.5	3.1 ± 0.3	0.37 ± 0.07
Brequinar	3.8 ± 0.9	0.46 ± 0.05	0.69 ± 0.07	0.12 ± 0.02

^{a} IC_{50} represents the concentration of the drug inhibiting cell growth by 50% after 48 h of treatment. ^{b} IC_{50} expressed as the mean ± SEM.

hydrochlorides is not or only slightly detrimental to the antiproliferative activity. Moreover, HT-1080 cancer cells are the most sensitive cell line studied with IC_{50}, mostly in the low micromolar range, while MF7, M21 and HT-29 generally show similar lower sensitivity to PYRUB-SOs, with IC_{50} in the mid-micromolar range. In addition, the position of the nitrogen atom on the pyridinyl group located at position 3 (**1–11** and **19–29**) or 5 (**12–18** and **30–36**) does not generally affect their antiproliferative activity, suggesting that the position of the nitrogen atom has no significant effect on the antiproliferative activity of PYRUB-SOs on non-AML human cancer cell lines. In addition, the alkyl chain positioned on the urea group adjacent to the phenyl ring A of PYRUB-SOs also seems to have only a weak impact on the antiproliferative activity of PYRUB-SOs. Overall, the most potent PYRUB-SOs are substituted with either an ethyl or a

2-chloroethyl group, followed closely by those substituted with a propyl group. Finally, PYRUB-SOs bearing either an iodine atom or an isopropyl group on pyridinyl ring B exhibit the strongest antiproliferative activity on HT-1080 cells with IC_{50} ranging from 1.1 to 5.9 µM.

2.3.2 Antiproliferative activity of PYRUB-SOs on human AML cell lines. We subsequently evaluated the antiproliferative activity of PYRUB-SOs **1–36** on MOLM-13, THP-1 and HL-60 cell lines to assess the sensitivity of a panel of three human AML cell lines toward PYRUB-SOs. The IC_{50} values were obtained using the 3-(4,5-dimethylthiazol-2-yl)-2,5-diphenyltetrazolium bromide (MTT) colorimetric assay based on the ATCC protocol.[40] The MTT assay was used instead of the SRB assay because AML cell lines are non-adherent cells and are easier to handle for assays that do not require washing steps. The same controls as in previous

Table 3 Antiproliferative activity (IC_{50}) of PYRUB-SOs **1–18**, their hydrochloride salts **19–36**, SFOM-0046 and brequinar on MOLM-13, THP-1 and HL-60 human AML cell lines

Compound	$IC_{50}{}^{a}$ (µM) ± SEM^{b}		
	MOLM-13	THP-1	HL-60
1	1.1 ± 0.2	7 ± 1	40 ± 10
2	0.9 ± 0.3	3.8 ± 0.6	25 ± 4
3	0.8 ± 0.2	1.5 ± 0.3	29 ± 6
4	6 ± 2	4.4 ± 0.2	50 ± 10
5	2.6 ± 0.1	5.9 ± 0.5	19 ± 2
6	2.2 ± 0.3	2.4 ± 0.1	24 ± 5
7	2.3 ± 0.5	2.6 ± 0.6	24 ± 4
8	13 ± 3	3.5 ± 0.9	35 ± 7
9	2.6 ± 0.8	1.2 ± 0.5	12 ± 1
10	1.5 ± 0.4	1.0 ± 0.1	6.9 ± 0.3
11	2.8 ± 0.4	2.3 ± 0.9	27 ± 6
12	2.5 ± 0.4	4.0 ± 0.6	>50
13	1.1 ± 0.2	1.8 ± 0.5	25 ± 7
14	3.0 ± 0.3	6 ± 2	>100
15	3.8 ± 0.6	6 ± 1	21 ± 5
16	1.3 ± 0.3	1.5 ± 0.4	18 ± 4
17	4.0 ± 0.6	7.3 ± 0.8	43 ± 7
18	0.6 ± 0.1	1.2 ± 0.3	3 ± 1
19	1.9 ± 0.5	7 ± 3	>100
20	0.8 ± 0.2	1.1 ± 0.5	37 ± 6
21	0.9 ± 0.2	6 ± 2	50 ± 10
22	9.7 ± 0.6	5 ± 2	60 ± 20
23	5 ± 1	10.0 ± 0.3	37 ± 7
24	3.7 ± 0.9	3.9 ± 0.7	30 ± 10
25	1.9 ± 0.5	2.4 ± 0.9	8 ± 3
26	14 ± 2	6 ± 2	15 ± 3
27	4.8 ± 0.7	4.9 ± 0.3	>50
28	2.4 ± 0.4	1.8 ± 0.7	19 ± 4
29	2.5 ± 0.9	2.6 ± 0.9	13 ± 4
30	3.7 ± 0.5	6 ± 2	80 ± 5
31	1.4 ± 0.4	2.2 ± 0.3	32 ± 9
32	2.4 ± 0.3	2.9 ± 0.1	>100
33	6 ± 1	4.1 ± 0.7	40 ± 10
34	2.7 ± 0.5	2.1 ± 0.6	>50
35	9.2 ± 0.8	5 ± 2	16.3 ± 0.1
36	0.7 ± 0.2	0.9 ± 0.2	3 ± 1
SFOM-0046	0.7 ± 0.2	4 ± 1	10 ± 1
Brequinar	0.1 ± 0.02	0.17 ± 0.04	1.2 ± 0.2

^{a} IC_{50} represents the concentration of the drug inhibiting cell growth by 50% after 48 h of treatment. ^{b} IC_{50} expressed as the mean ± SEM.

experiments using non-AML adherent human tumour cell lines were used. The results reported in Table 3 show a comparable general trend of SARs on AML cells and non-AML cells. Firstly, the antiproliferative activity of PYRUB-SOs and their hydrochlorides is comparable and within the same order of magnitude as that of PUB-SOs.[27] However, the IC_{50} of PYRUB-SOs indicates slightly lower potency compared to their PUB-SO counterparts, suggesting that the substitution of the phenyl ring B in PUB-SOs with a pyridinyl group exerts only a minimal impact on the antiproliferative efficacy against AML cells. Secondly, the most potent PYRUB-SOs are generally the ones bearing an iodo or an isopropyl substituent on the pyridinyl ring and having either an ethyl or a 2-chloroethyl chain grafted on the urea moiety. Thirdly, the nitrogen atom's position doesn't alter the antiproliferative activity of PYRUB-SOs. The most sensitive AML cell line to PYRUB-SOs is MOLM-13 (0.6 µM to 14 µM) followed by THP-1 (0.9 µM to 10 µM) with IC_{50} values in the low micromolar range that are generally more sensitive than the most sensitive non-AML cell line HT-1080. The least sensitive AML cell line is HL-60 (3 µM to >100 µM) with most compounds exhibiting antiproliferative activity in the higher micromolar range (>10 µM), which follows the same trends as our previous SAR studies on PUB-SOs. Finally, PYRUB-SOs **2** and **3** together with their corresponding hydrochlorides **20** and **21** were chosen for subsequent biological evaluation for their promising antiproliferative activity on non-AML and AML cells and their higher water solubility.

2.3.3 PYRUB-SOs induce cell cycle arrest in M21 and AML cells. Our previous studies established that PUB-SOs bearing an ethyl or 2-chloroethyl chain and substituted by either an iodo or an isopropyl group induced cell cycle arrest in the S-phase.[24,25] Moreover, the cell cycle progression arrest in S-phase is a prerequisite for DHODH inhibition. We thus assessed the effect of PYRUB-SOs **2** and **3**, and their corresponding hydrochlorides **20** and **21**, on the cell cycle progression of M21 and AML MOLM-13 and THP-1 cells that were the most sensitive to the antiproliferative activity of PYRUB-SOs. The cancer cells were treated with PYRUB-SOs for 24 h at either 2- or 5-fold their corresponding IC_{50}. SFOM-0046 and brequinar were used as positive controls, while DMSO was used as an excipient. As shown in Fig. 2–4, PYRUB-SOs **2** and **3** and their hydrochlorides **20** and **21** significantly arrest the cycle progression of all cells tested (M21 and AML cells) in the S-phase. Indeed, PYRUB-SOs **2**, **3**, **20** and **21** increase the number of cells in S-phase by 17 to 24%, 14 to 31% and 15 to 23% for M21, MOLM-13 and THP-1 cells, respectively, compared to the S-phase of the same cell lines sham-treated with DMSO (20, 25 and 16%). These increases are comparable to or exceeded those observed with SFOM-0046 and brequinar (25–30, 16–51 and 13–43% for M21, MOLM-13 and THP-1 cells, respectively). These findings validate the potential of PYRUB-SOs to impede the cell cycle progression of M21 and AML cells in S phase.

2.3.4 PYRUB-SOs induce the phosphorylation of the histone H2AX. Our previous studies on PUB-SOs evidenced

that PUB-SOs blocking the cell cycle progression in the S-phase induce the phosphorylation of H2AX into γH2AX, an important marker of replication stress.[24,25] Therefore, to corroborate the replication stress induced by PYRUB-SOs, the effect of PYRUB-SOs **2**, **3**, **20** and **21** on H2AX phosphorylation was evaluated on M21 cells by immunofluorescence after 24 h of treatment at 2-fold their respective IC_{50}. As shown in Fig. 5, γH2AX foci were stained in red while nuclei were stained in blue with 4′,6-diamidino-2-phenylindole (DAPI). SFOM-0046 and brequinar were used as positive controls, and DMSO (0.5%) was used as the excipient. Our results indicate that PYRUB-SOs promote the phosphorylation of H2AX into γH2AX, as substantiated by the elevated quantity of γH2AX foci in PYRUB-SO-treated cells compared to sham-treated cells with DMSO which had minimal or no γH2AX foci. The induction of γH2AX foci by PYRUB-SOs is comparable to that of the positive controls SFOM-0046 and brequinar. These results suggest that PYRUB-SOs trigger replicative stress leading to the arrest of the cell cycle progression in S-phase. The inhibition of DHODH, the putative target of PYRUB-SOs, may potentially cause this cellular response.

2.3.5 PYRUB-SOs inhibit DHODH activity. To confirm that PYRUB-SOs are DHODH inhibitors, the most potent and water-soluble PYRUB-SO hydrochlorides **20** and **21** were evaluated in the human DHODH colorimetric inhibition assay based on the procedure reported by Bouzriba *et al.*[26] The assay relies on the conversion of dihydroorotate (DHO) to orotate by DHODH which reduces the blue-color 2,6-dichlorophenolindophenol (DCIP) into its reduced 2,6-dichlorophenolindophenol (DCIPH$_2$) colorless product. The activity of DHDOH correlates to the reduction of DCIP to DCIPH$_2$, which is measured using UV absorbance spectroscopy. Results shown in Fig. 6 evidence that PYRUB-SOs **20** and **21** inhibit DHODH activity with IC_{50} of 31 and 12 nM, respectively. The IC_{50} of both PYRUB-SOs parallel those of SFOM-0046 and brequinar (IC_{50} of 72 and 12 nM, respectively). These results confirm that DHODH is a pharmacological target of PYRUB-SOs, analogous to their PUB-SO counterparts. These results suggest that inhibition of DHODH in the *de novo* pyrimidine biosynthesis pathway by PYRUB-SOs is the direct cause of replicative stress shown by the induction of the H2AX phosphorylation and cell cycle arrest in the S-phase.

2.3.6 PYRUB-SOs dock into the brequinar-binding site of DHODH. Molecular docking studies of PYRUB-SOs **20** and **21** were performed using the Molecular Operating Environment (MOE) drug discovery software platform to confirm their binding affinity to the brequinar-binding site of DHODH. The X-ray crystallographic structure of DOHDH complexed to 6-fluoro-2-[2-methyl-4-phenoxy-5-(propan-2-yl)phenyl]quinoline-4-carboxylic acid (C44), a brequinar analog (ID: 4IGH at 1.3 Å resolution) was obtained from the RCSB protein data bank and loaded to MOE software. The brequinar-binding site is constituted of 39 amino acids and flavin mononucleotide (FMN). The most favorable poses of PYRUB-SOs **20** and **21** in
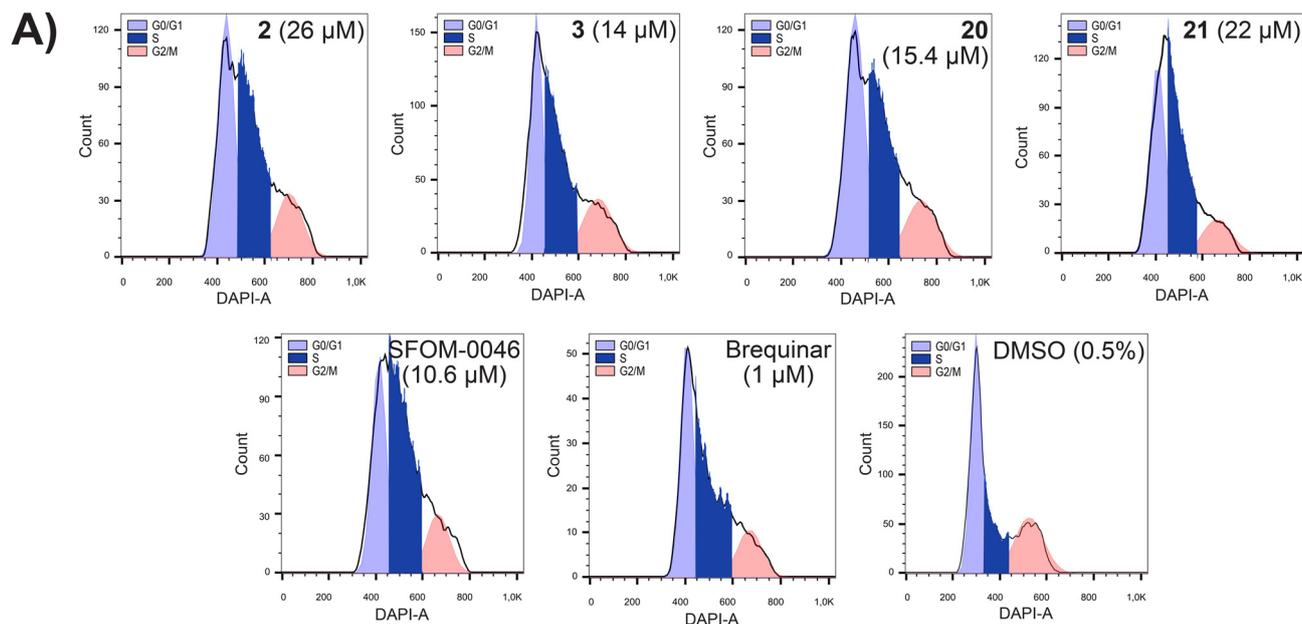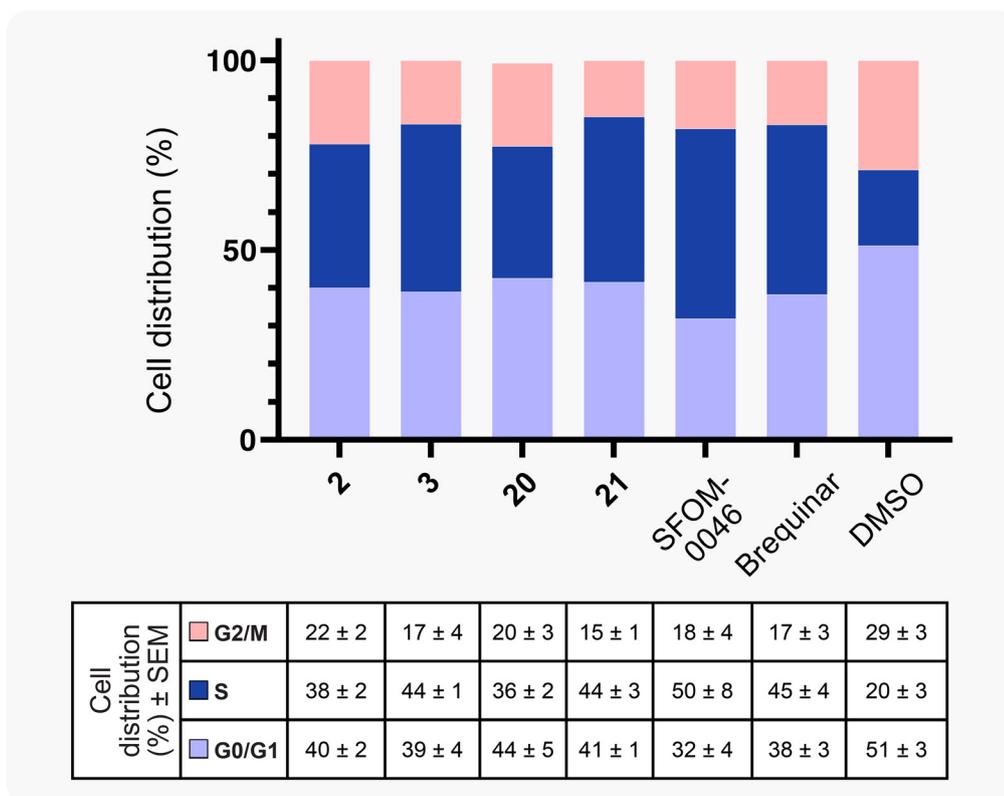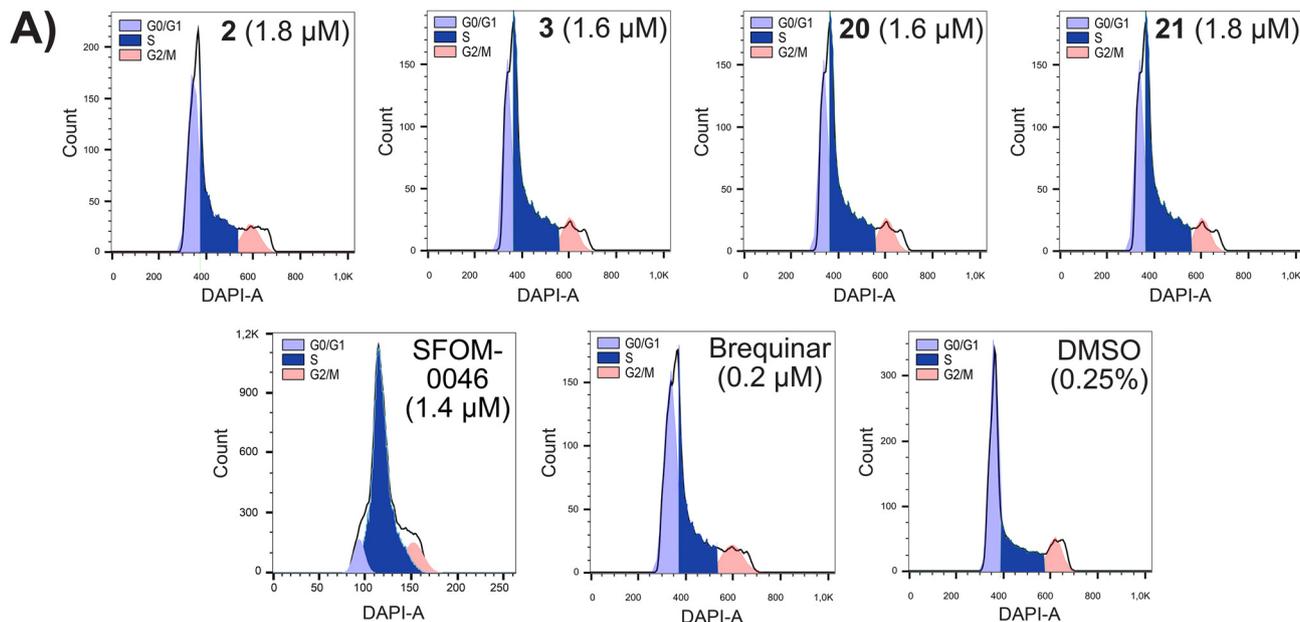
Fig. 2 A) Effects of PYRUB-SOs **2** and **3** and their corresponding hydrochlorides **20** and **21** on the cell cycle progression of non-AML M21 cells. SFOM-0046 and brequinar were used as positive controls, while 0.5% DMSO was used as the excipient. B) Histogram displaying cell cycle distribution.

the brequinar-binding site stacked with brequinar analog C44 are illustrated in Fig. 7A and B, while the energy docking results of the top 5 poses are collated Table 4. Our results show that the most favorable poses for compounds **20** and **21** exhibit S energy scores of −7.85 and −7.73 kcal mol^{-1}, respectively. Moreover, our findings indicate that PYRUB-SOs

dock into the brequinar-binding site similarly to C44 by occupying identical positions. Furthermore, Fig. 7C and D display the 2D interaction diagram of PYRUB-SOs **20** and **21** with the brequinar-binding site. As illustrated, PYRUB-SO **20** has 3 interactions with the binding site, while PYRUB-SO **21** displays only one interaction. On the one hand, PYRUB-SO **20**
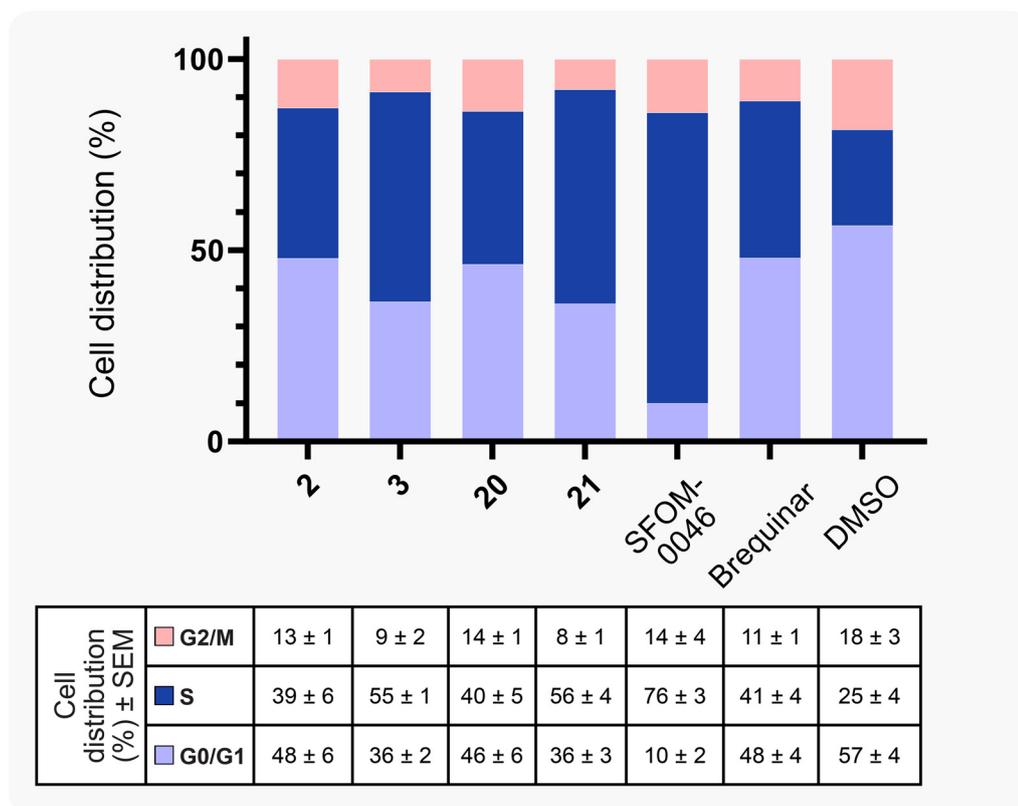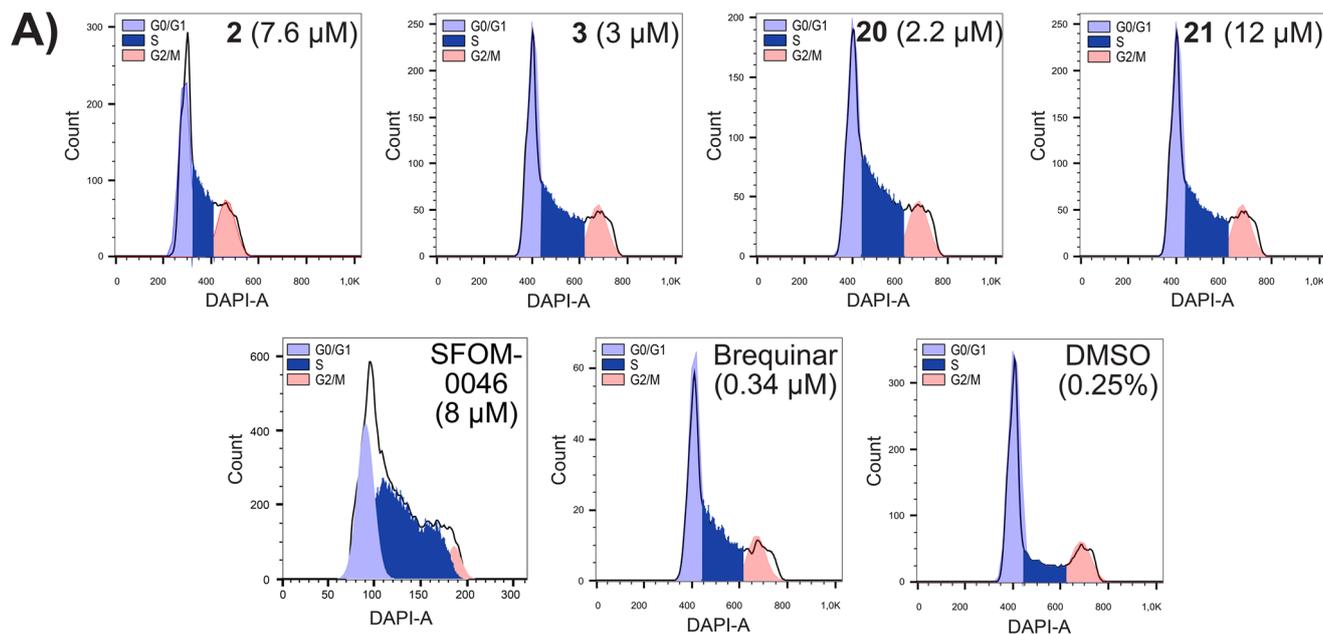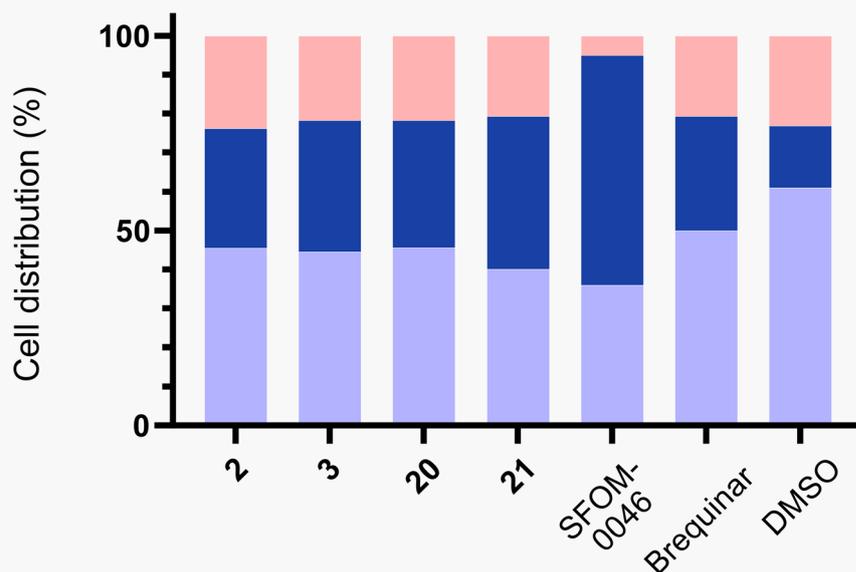
Fig. 3 A) Effects of PYRUB-SOs 2 and 3 and their corresponding hydrochlorides 20 and 21 on the cell cycle progression of AML MOLM-13 cells. SFOM-0046 and brequinar were used as a positive control, while 0.25% DMSO was used as the excipient. B) Histogram displaying cell cycle distribution.

forms an H-donor interaction with Leu67 through the carbon adjacent to the nitrogen atom on the pyridinyl moiety, and both phenyl and pyridinyl groups form a pi–H interaction with Phe62 and Thr360, respectively. On the other hand, PYRUB-SO 21 forms a pi–H interaction through the methyl alongside the urea group with His56. In summary, our docking studies demonstrated that PYRUB-SOs 20 and 21 possess the molecular properties for efficient interaction with the brequinar-binding site on DHODH. The results showcase the potential active conformation of the PYRUB-SOs and highlight their significant interactions with key amino acids critical for optimal biological activity.

Fig. 4 A) Effects of PYRUB-SOs **2** and **3** and their corresponding hydrochlorides **20** and **21** on the cell cycle progression of AML THP-1 cells. SFOM-0046 and brequinar were used as positive controls, while 0.25% DMSO was used as the excipient. B) Histogram displaying cell cycle distribution.

Cell distribution (%) ± SEM		2	3	20	21	SFOM-0046	Brequinar	DMSO
	G2/M	24 ± 1	22 ± 2	22 ± 1	21 ± 1	5 ± 1	21 ± 4	23 ± 3
	S	31 ± 1	34 ± 4	33 ± 1	39 ± 3	59 ± 1	29 ± 8	16 ± 4
	G0/G1	45 ± 3	44 ± 2	45 ± 1	40 ± 1	36 ± 2	50 ± 4	61 ± 3

2.3.7 PYRUB-SOs induce cell differentiation of AML cells. PUB-SOs and DHODH inhibitors are known to differentiate AML cell lines. In this context, the effect of PYRUB-SOs **20** and **21** as potent DHODH inhibitors was evaluated on the induction of differentiation in AML cell lines MOLM-13 and THP-1. Flow cytometry was used to monitor the expression of myeloid differentiation markers CD11b and CD14 after 120 h of treatment of PYRUB-SOs **20** and **21** at 2-fold their respective IC_{50}. SFOM-0046 and brequinar at 2-fold their respective IC_{50} were used as positive controls while DMSO
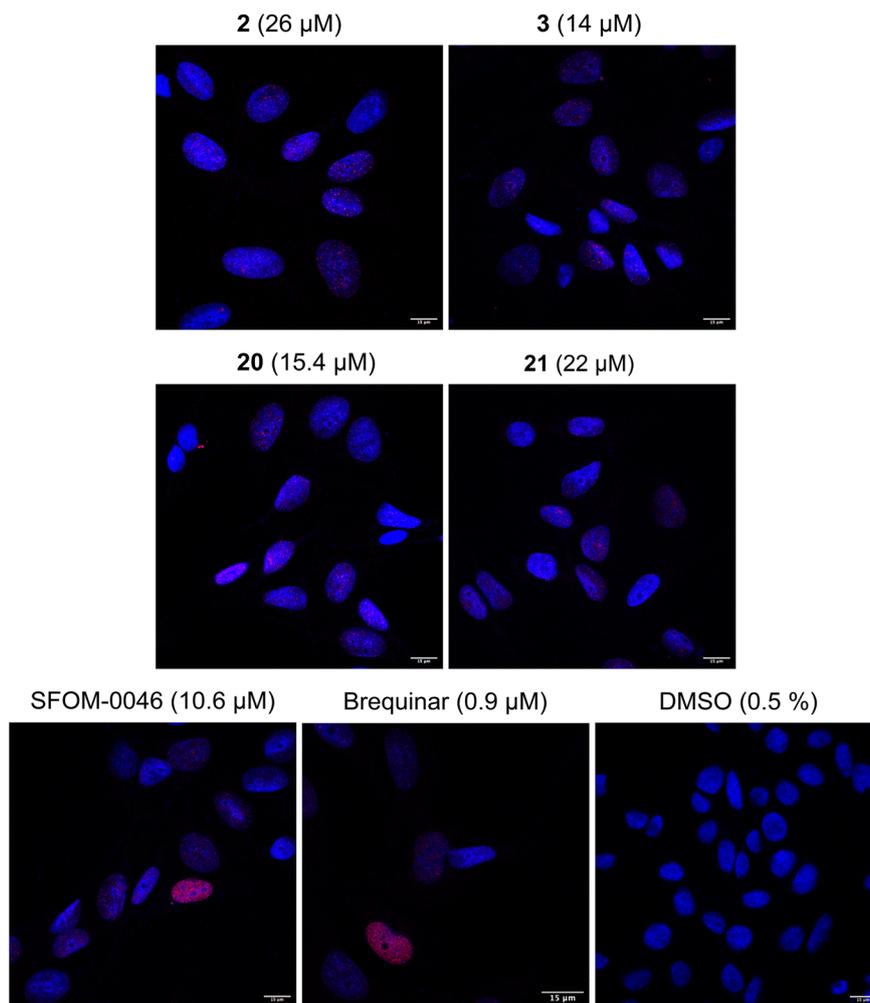
Fig. 5 Effects of PYRUB-SOs **2** and **3** and their corresponding hydrochlorides **20** and **21** on the induction of the phosphorylation of H2AX into γH2AX in M21 cells after an incubation period of 24 h. SFOM-0046 and brequinar served as positive controls, and DMSO as the excipient.
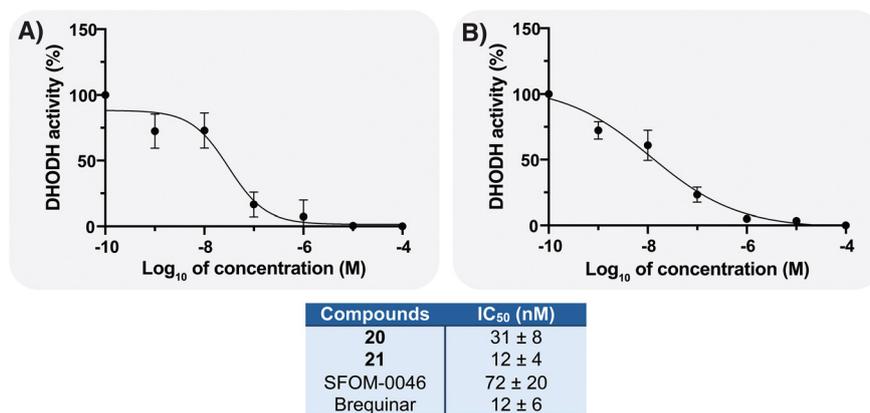

Compounds	IC_{50} (nM)
20	31 ± 8
21	12 ± 4
SFOM-0046	72 ± 20
Brequinar	12 ± 6

Fig. 6 Inhibition of DHODH by PYRUB-SOs A) **20** and B) **21**. IC_{50} of SFOM-0046 and brequinar were previously reported by Bouzriba *et al.*[26] IC_{50} is expressed as the mean ± SEM.

(0.1%) served as excipient. Our results show that PYRUB-SOs **20** and **21** induce CD11b expression in 38 and 26% of the cell population in MOLM-13 cells, while SFOM-0046 and brequinar used as positive controls induce CD11b expression in 38 and 34% of the cells, respectively (Fig. 8). Interestingly, and as shown in Fig. 9, PYRUB-SO **21** induced both CD11b
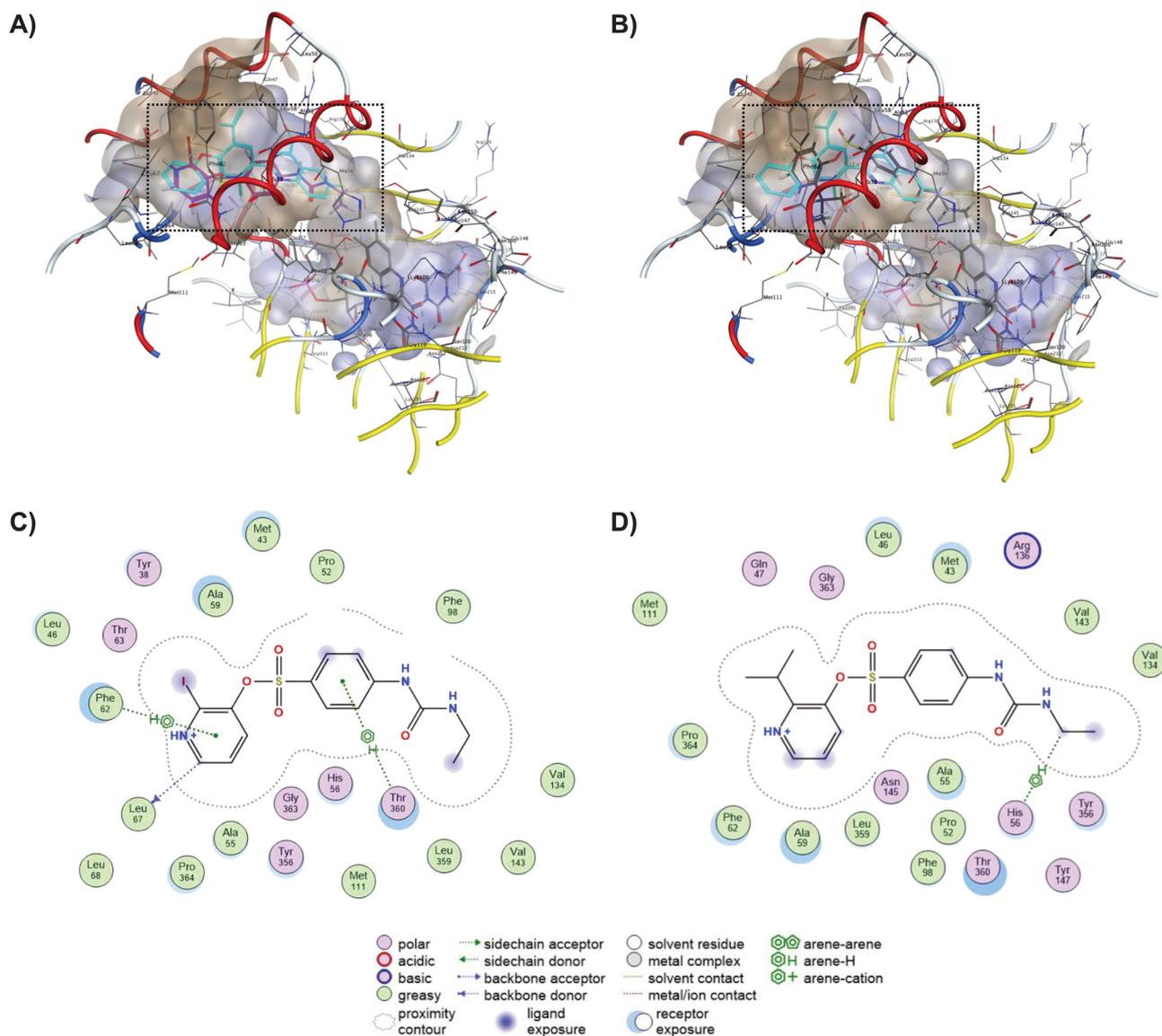
Fig. 7 Docking of the most stable conformation of PYRUB-SOs A) **20** (purple) and B) **21** (black) stacked with brequinar analog C44 (cyan) in the brequinar-binding site. 2D interaction of the most stable poses of PYRUB-SOs C) **20** and D) **21** in the brequinar-binding site.

Table 4 Docking energy of the 5 most favorable poses of PYRUB-SOs **20** and **21** in the brequinar-binding site

Pose	PYRUB-SO **20**		PYRUB-SO **21**	
	S^a (kcal mol^{-1})	RMSD^b refine (Å)	S^a (kcal mol^{-1})	RMSD^b refine (Å)
1	−7.85	1.41	−7.73	1.50
2	−7.69	1.31	−7.72	1.05
3	−7.66	1.86	−7.58	0.91
4	−7.65	2.32	−7.57	1.60
5	−7.62	1.61	−7.56	1.88

^{a} S: entropy. ^{b} RMSD: root-mean-square deviation.

and CD14 positivity in 57% of the THP-1 cell population. The double-positive differentiation indicates a more advanced differentiation of this cell population. This prompted us to determine the relative half-maximal effective concentration

(EC_{50}) of PYRUB-SOs **20** and **21** on THP-1 cells, defined as the concentration required to achieve 50% of the observed maximal effect under the experimental conditions. Our results show that PYRUB-SOs **20** and **21** induced CD11b and
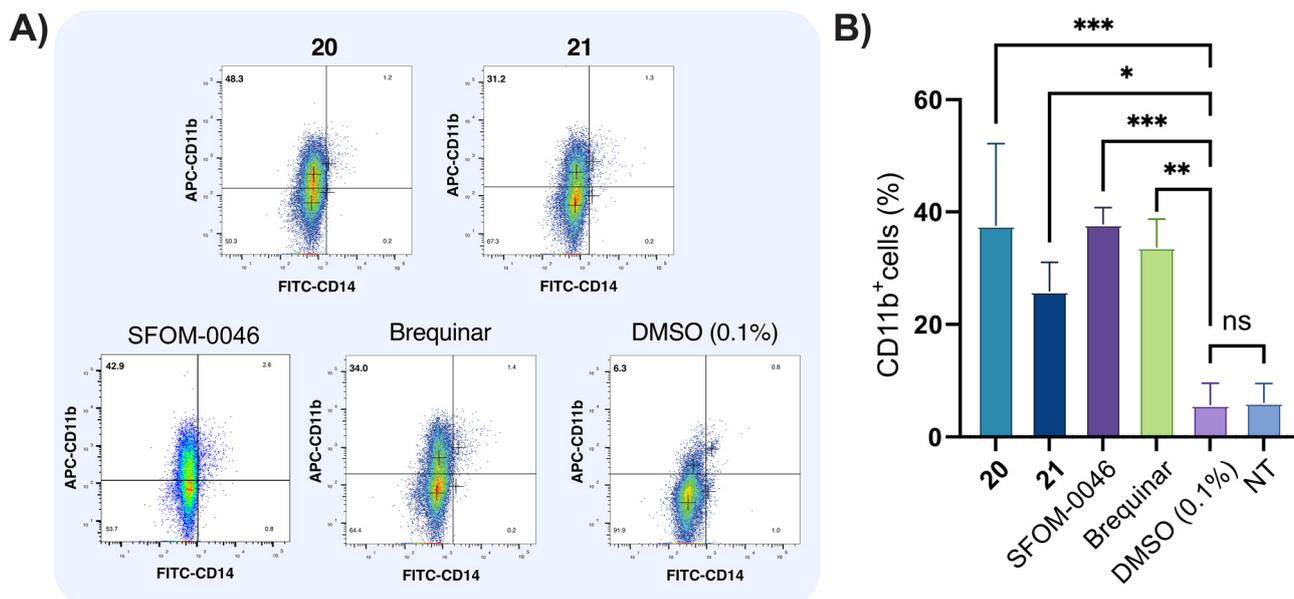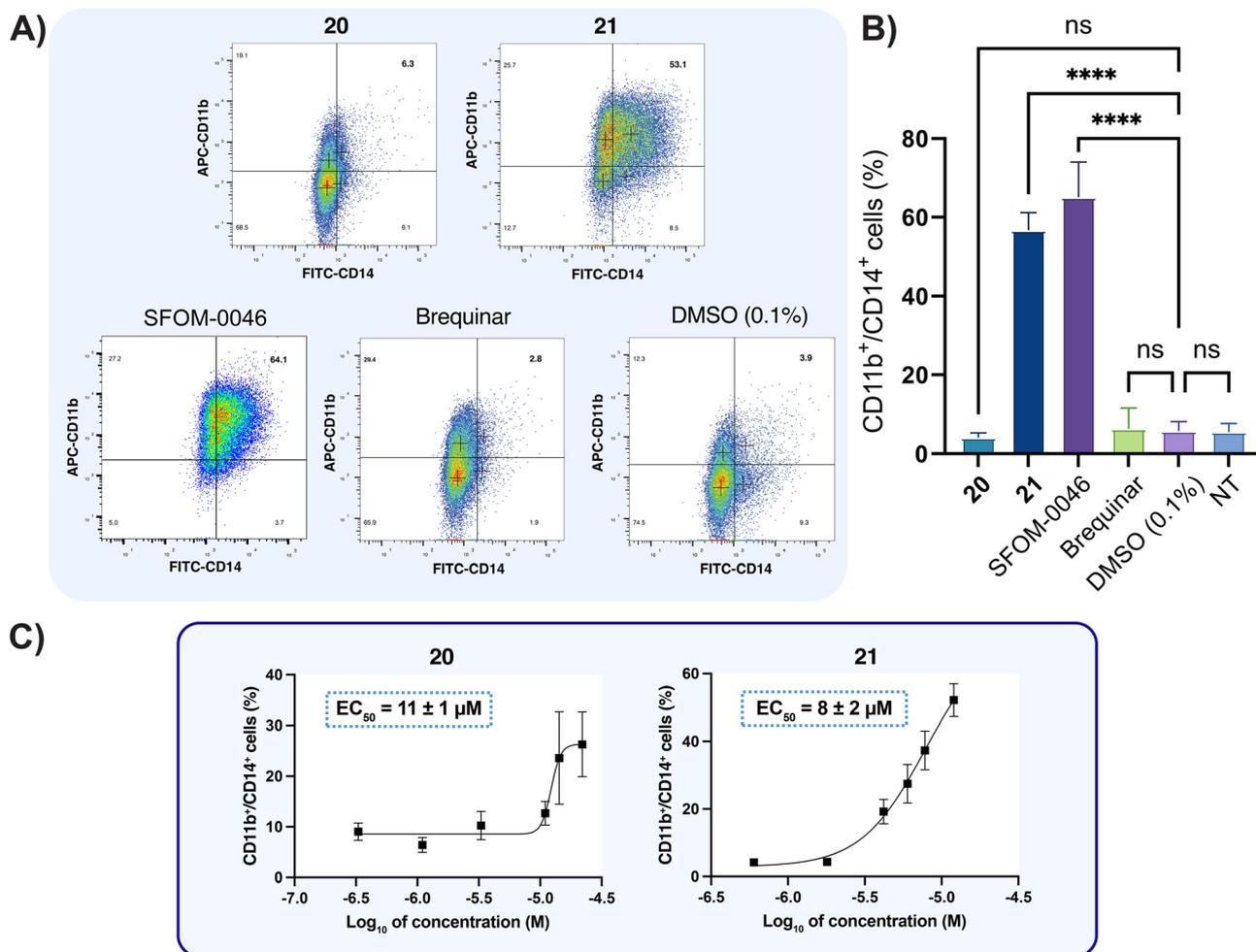
Fig. 8 Induced differentiation by PYRUB-SOs **20** and **21** on MOLM-13 cells. SFOM-0046 and brequinar were used as positive controls, while DMSO (0.1%) was used as the excipient. A) Representative scatter plots and B) histograms summarizing the CD11b$^+$ cell population. Statistical significance: *$p \leq 0.05$; **$p \leq 0.01$; ***$p \leq 0.001$.

CD14 double-positive differentiation with EC$_{50}$ of 11 and 8 μM, respectively. These results strongly suggest that PYRUB-SOs act as differentiation agents for AML MOLM-13 and THP-1 cells through their DHODH inhibition.

2.3.8 Metabolic stability of PYRUB-SOs in rodent and human liver microsomes. The metabolic stability of PYRUB-SOs **20** and **21** was evaluated on mouse (MLM), rat (RLM) and human (HLM) liver microsomes. PYRUB-SOs **20** and **21** were incubated with liver microsomes to determine their metabolic profile. Their half-lives ($t_{1/2}$) and their intrinsic clearances (CL$_{ints}$) were calculated after UHPLC analysis. Results are compiled in Table 5 and show that the $t_{1/2}$ of PYRUB-SOs increases with animal species. The $t_{1/2}$ were 80 and 57 min when using MLM, 190 and 150 min for RLM and 216 and 89 min for HLM, for compounds **20** and **21**, respectively. CL$_{ints}$ were then calculated from the $t_{1/2}$ with values of 18 and 25 μL min^{-1} mg^{-1} of protein for MLM, 7.4 and 11 μL min^{-1} mg^{-1} of protein from RLM and 6.5 and 15.7 μL min^{-1} mg^{-1} of protein for HLM for PYRUB-SOs **20** and **21**, respectively. These results can be ranked by their clearance in either low, medium or high clearance categories.[41] Both compounds are in the medium clearance category for MLM ($13.1 < CL_{int} < 71.1$) and in the low clearance category for RLM ($CL_{int} < 15.8$). For HML, compound **20** falls in the low clearance category ($CL_{int} < 8.61$) while compound **21** is in the medium clearance category ($8.6 < CL_{int} < 47.0$). Our results indicate that PYRUB-SO **20** has a slightly better metabolic stability than PYRUB-SO **21**. Nevertheless, these results strongly indicate that both PYRUB-SOs possess metabolic profiles appropriate for animal studies and that substituting the phenyl ring B with a pyridinyl group in the molecular structure of PUB-SOs preserves their favorable metabolic stability.

2.3.9 PYRUB-SOs have favorable pharmacokinetic, physicochemical and drug likeness properties. The in silico ADME properties of PYRUB-SOs **2** and **3** were predicted using the open-access software SwissADME. The latter is a tool designed to evaluate small molecules' pharmacokinetic, drug-likeness and physicochemical properties.[28] This evaluation allows us to predict and assess the effects of substituting aromatic rings with pyridinyl groups on various theoretical biopharmaceutical properties of PUB-SOs. We evaluated the corresponding PYRUB-SOs **2** and **3** instead of their hydrochlorides **20** and **21** since the computational model is only reliable for predicting neutral molecules, as using ionized molecules can lead to significant biases in the modeling results.[42] Results from the analysis are summarized in Table 6. First, the physicochemical properties evaluated show that PYRUB-SOs **2** and **3** have molecular weights of 447.25 and 363.43 g mol^{-1}, respectively; both bear 5 H-bond acceptors and 2 H-bond donors and have 7 and 8 rotatable bonds, respectively. Moreover, both PYRUB-SOs display acceptable topological polar surface area (TPSA) having a TPSA value of 105.77 Å^2, indicating good permeability in cellular membranes.[43] The water solubility of PYRUB-SOs **2** and **3** is predicted to be moderately soluble, which correlates with the results obtained by our solubility assay. Furthermore, they display suitable lipophilicity with clog P values of 2.26 and 2.52 for PYRUB-SOs **2** and **3**, respectively. The lipophilicity influences drug solubility and permeability; thus, drugs with higher lipophilicity (log $P > 5$) tend to exhibit high metabolic rates, poor solubility, and low absorption.[44] With these results for physicochemical properties, PYRUB-SOs **2** and **3** respect Lipinski rule of 5 as well as the other drug-likeness filters, such as Veber, Muegge,

Fig. 9 Induced differentiation by PYRUB-SOs **20** and **21** on THP-1 cells. SFOM-0046 and brequinar were used as positive controls, while DMSO (0.1%) was used as the excipient. A) Representative scatter plots, B) histograms summarizing the CD11b$^+$/CD14$^+$ cell population in treated THP-1 and C) EC$_{50}$ of PYRUB-SOs **20** and **21**. Statistical significance: ****$p \leq 0.0001$.

Table 5 Half-life ($t_{1/2}$) and intrinsic clearance (CL$_{int}$) of PYRUB-SO hydrochlorides **20** and **21** when incubated with mouse (MLM), rat (RLM) or human liver microsomes (HLM)

Compound	Half-life ($t_{1/2}$)^a (min)			Intrinsic clearance (CL$_{int}$)^a (μL min^{-1} mg^{-1} of protein)		
	MLM	RLM	HLM	MLM	RLM	HLM
20	80 ± 10	190 ± 20	216 ± 10	18 ± 2	7.4 ± 0.6	6.5 ± 0.3
21	57 ± 4	150 ± 30	89 ± 2	25 ± 2	11 ± 2	15.7 ± 0.3

^{a} The $t_{1/2}$ and CL$_{int}$ represent the mean of three independent experiments, and the errors are expressed as SEM.

Egan and Ghose, having no violations, indicating favorable properties for increased bioavailability. Furthermore, pharmacokinetic parameters such as gastrointestinal absorption (GIA), and blood–brain-barrier permeability (BBB) were evaluated. Results predict that both PYRUB-SOs have high gastrointestinal absorption and are not BBB permeant, suggesting they would be easily absorbed by the GI tract without inducing unwanted toxicity to the brain through the BBB. Finally, the model predicts that PYRUB-SOs are not

substrates for P-glycoprotein (P-gp), suggesting a low likelihood of those compounds being effluxed from the cells by these proteins, which are major contributors to the tumour multidrug resistance.[45,46] Overall, the SwissADME analysis suggests that PYRUB-SOs hold favorable theoretical pharmacokinetic, physicochemical and drug-like properties, along with appropriate hepatic stability results, making them promising candidates for further *in vivo* experiments as potent DHODH acting as AML differentiation agents.

Table 6 Physicochemical, pharmacokinetic and druglikeness properties of PYRUB-SOs **2** and **3** are calculated by the SwissADME web tool

Properties	PYRUB-SO 2	PYRUB-SO 3
MW[a]	447.25	363.43
Rb[b]	7	8
H-Ba[c]	5	5
H-Bd[d]	2	2
TPSA (Å^2)[e]	105.77	105.77
clog P[f]	2.26	2.52
log S[g]	−3.86	−4.35
Sclass[h]	MS	MS
GIA[i]	High	High
BBB[j]	No	No
P-gp[k]	No	No
Drug-like (#viol.)[l]	Yes (0)	Yes (0)

[a] MW: molecular weight. [b] Rb: number of rotatable bonds. [c] H-Ba: number of H-bond acceptors. [d] H-Bd: number of H-bond donors. [e] TPSA: topological polar surface area. [f] clog P: consensus log P (average of iLOGP, XLOGP3, WLOGP, MLOGP and Silicos-IT Log P). [g] log S: Ali topological method log S. [h] SClass: Ali solubility class (insoluble (IS) < −10 < poorly soluble (PS) < −6 < moderately soluble (MS) < −4 < soluble (S) < −2 < very soluble (VS) < 0 < highly soluble (HS)). [i] GIA: gastrointestinal absorption (H means high). [j] BBBP: blood–brain barrier permeability. [k] P-gp: P-glycoprotein substrates. [l] Drug-like: drug likeness (bioavailability) from Lipinski, Ghose, Veber, Egan, and Muegge filters. # viol: number of violations of the five filters.

3 Conclusion

To conclude, we have successfully designed, synthesized, characterized and biologically evaluated a series of 18 novel PYRUB-SO derivatives along with their hydrochloride salts. Our results indicate that replacing the phenyl ring B of PUB-SOs with pyridinyl groups and forming their respective hydrochloride salt improves the water solubility of original PUB-SOs by up to 42-fold. PYRUB-SOs bearing either an iodo or an isopropyl group exhibit antiproliferative activity in the micromolar range on various non-AML and AML cancer cell lines. The most potent PYRUB-SOs **2** and **3** and their hydrochlorides **20** and **21** induce cell arrest in the S-phase and phosphorylation of H2AX into γH2AX. Moreover, DHODH inhibition assays evidenced that PYRUB-SOs **20** and **21** act as potent DHODH inhibitors and *in silico* docking studies suggest that they bind to the brequinar-binding site of DHODH. Furthermore, PYRUB-SOs **20** and **21** induce the differentiation of AML cells in both MOLM-13 and THP-1 cell lines. Additionally, PYRUB-SOs exhibit good metabolic stability in rodents and human microsomes. They also possess theoretical physicochemical, pharmacokinetic and drug likeness properties suitable for animal studies. Importantly, our study highlights that the formation of hydrochloride salts enhances their water solubility without compromising their biological activity. This improvement is of the utmost importance for increasing the concentration of PYRUB-SOs in the excipients used for either biofunctional assays or for further studies on animal models. Our results also showcase that pyridinyl groups are effective bioisosteric

equivalents of the phenyl ring B of PUB-SOs, making PYRUB-SOs a promising novel family of DHODH inhibitors for AML treatment.

4 Experimental section

4.1 Chemistry

4.1.1 General. All chemicals and solvents were purchased for commercial suppliers and used without further purification. ^{1}H and ^{13}C NMR spectra were recorded on a Bruker AM-300 spectrometer (Bruker, Germany) at 300 MHz and all spectra were taken in deuterated dimethyl sulfoxide (DMSO-d$_6$). Chemical shifts (δ) are reported in parts per million (ppm). The following abbreviations report NMR multiplicities: s, singlet; t, triplet; q, quartet; quint, quintet; sext, sextet; m, multiplet. High-resolution mass spectrometry (HRMS) spectra were recorded on a time-of-flight (TOF) system 6210 series mass spectrometer (Agilent Technologies, Santa Clara, CA, USA) by direct injection using electrospray ionization (ESI). Uncorrected melting points were acquired on a MPA100 automated melting point system (SRS Stanford Research Systems, Sunnyvale, CA, USA). Reaction progress was checked by thin-layer chromatography (TLC) on precoated silica gel 60 Å F254 TLC plates and visualized under UV light at 254 nm. Compounds were purified on an FPX flash purification system (Biotage, Charlottesville, VA, USA) using silica gel F60, 60 Å, 40–63 μm, supplied by Silicycle (Quebec City, QC, Canada) with solvent gradients expressed as v/v ratio. UHPLC analyzes were conducted using an ACQUITY Arc system (Waters, Mississauga, ON, Canada) coupled with a 2998 UV-visible photodiode array (PDA) detector on a CORTECS C18+ silica-based reserved-phase column (90 Å, 3.0 × 50 mm × 2.7 μm) equipped with a CORTECS C18+ VanGuard Cartridge (90 Å, 2.1 × 5 mm × 2.7 μm). Samples were eluted with a linear gradient of H$_2$O/MeOH (1/1) at 1.0 mL min^{-1}. Samples were detected at a wavelength of 280 nm. Purity was ≥95% for all compounds tested.

4.1.2 General preparation of PYRUB-SOs 1–18. The relevant pyridinol (1.5 eq., 1.5 mmol) was added to a solution of appropriate ureidobenzenesulfonyl chloride (**40–42**, 1 mmol, 1.0 eq.) in the presence of triethylamine (3 mmol, 3.0 eq.) in methylene chloride (10 mL). The reaction mixture was stirred at room temperature for 48 h. After the completion of the reaction, the organic layer was washed successively with a solution of sodium hydroxide 1 M and thrice with brine, dried with anhydrous sodium sulfate, filtered and evaporated under reduced pressure. The residue was purified by flash chromatography to afford the desired PYRUB-SO.

4.1.3 Characterization of PYRUB-SOs 1–18

4.1.3.1 2-Bromopyridin-3-yl 4-(3-ethylureido)benzenesulfonate (1). Flash chromatography (methylene chloride to methylene chloride/EtOAc (90:10)). Yield: 66%; white solid; mp: 131–133 °C. ^{1}H NMR (DMSO-d$_6$): δ 9.18 (s, 1H, NH), 8.34–8.31 (m, 1H, Ar), 7.72–7.62 (m, 5H, Ar), 7.54–7.49 (m, 1H, Ar), 6.38 (t, *J* = 5.6 Hz, 1H, NH), 3.10 (quint, *J* = 7.0 Hz, 2H, CH$_2$), 1.04 (t, *J*

= 7.2 Hz, 3H, CH$_3$). ^{13}C NMR (DMSO-d$_6$): δ 154.8, 148.9, 147.7, 144.1, 136.3, 132.7, 130.5, 125.2, 124.6, 117.6, 34.5, 15.7. HRMS (ESI) m/z found, 399.9964; C$_{14}$H$_{15}$BrN$_3$O$_4$S (M$^+$ + H) expected, 399.9967.

4.1.3.2 2-Iodopyridin-3-yl 4-(3-ethylureido)benzenesulfonate (2). Flash chromatography (methylene chloride to methylene chloride/EtOAc (90 : 10)). Yield: 53%; white solid; mp: 165–167 °C. ^{1}H NMR (DMSO-d$_6$): δ 9.18 (s, 1H, NH), 8.30–8.28 (m, 1H, Ar), 7.74–7.62 (m, 4H, Ar), 7.57–7.54 (m, 1H, Ar), 7.48–7.43 (m, 1H, Ar), 6.38 (t, J = 5.6 Hz, 1H, NH), 3.10 (quint, J = 7.2 Hz, 2H, CH$_2$), 1.04 (t, J = 7.2 Hz, 3H, CH$_3$). ^{13}C NMR (DMSO-d$_6$): δ 163.8, 154.8, 149.7, 147.7, 130.6, 130.4, 124.9, 124.8, 117.5, 116.6, 34.5, 15.7. HRMS (ESI) m/z found, 447.9821; C$_{14}$H$_{15}$IN$_3$O$_4$S (M$^+$ + H) expected, 447.9828.

4.1.3.3 2-Isopropylpyridin-3-yl 4-(3-ethylureido) benzenesulfonate (3). Flash chromatography (methylene chloride to methylene chloride/EtOAc (90 : 10)). Yield: 39%; white solid; mp: 166–168 °C. ^{1}H NMR (DMSO-d$_6$): δ 9.15 (s, 1H, NH), 8.47–8.44 (m, 1H, Ar), 7.70–7.61 (m, 4H, Ar), 7.46–7.42 (m, 1H, Ar), 7.29–7.24 (m, 1H, Ar), 6.38–6.35 (m, 1H, NH), 3.15–3.06 (m, 3H, CH and CH$_2$), 1.06–0.95 (m, 9H, 3 × CH$_3$). ^{13}C NMR (DMSO-d$_6$): δ 159.7, 154.8, 148.3, 147.4, 143.3, 130.4, 130.2, 125.1, 122.8, 117.6, 34.5, 28.8, 21.9, 15.7. HRMS (ESI) m/z found, 364.1331; C$_{17}$H$_{22}$N$_3$O$_4$S (M$^+$ + H) expected, 364.1331.

4.1.3.4 2-Methylpyridin-3-yl 4-(3-ethylureido)benzenesulfonate (4). Flash chromatography (methylene chloride to methylene chloride/EtOAc (90 : 10)). Yield: 75%; white solid; mp: 110–112 °C. ^{1}H NMR (DMSO-d$_6$): δ 9.15 (s, 1H, NH), 8.37–8.36 (m, 1H, Ar), 7.69–7.61 (m, 4H, Ar), 7.43–7.40 (m, 1H, Ar), 7.30–7.25 (m, 1H, Ar), 6.39–6.35 (m, 1H, NH), 3.10 (quint, J = 7.1 Hz, 2H, CH$_2$), 2.14 (s, 3H, CH$_3$), 1.04 (t, J = 7.2 Hz, 3H, CH$_3$). ^{13}C NMR (DMSO-d$_6$): δ 154.8, 152.2, 148.0, 147.4, 144.7, 130.5, 130.2, 125.1, 123.1, 117.6, 34.5, 19.5, 15.7. HRMS (ESI) m/z found, 336.1020; C$_{15}$H$_{18}$N$_3$O$_4$S (M$^+$ + H) expected, 336.1018.

4.1.3.5 2-Bromopyridin-3-yl 4-(3-propylureido) benzenesulfonate (5). Flash chromatography (methylene chloride to methylene chloride/EtOAc (90 : 10)). Yield: 70%; white solid; mp: 139–141 °C. ^{1}H NMR (DMSO-d$_6$): δ 9.16 (s, 1H, NH), 8.34–8.32 (m, 1H, Ar), 7.72–7.61 (m, 5H, Ar), 7.54–7.50 (m, 1H, Ar), 6.42 (t, J = 5.7 Hz, 1H, NH), 3.04 (q, J = 6.5 Hz, 2H, CH$_2$), 1.43 (sext, J = 7.3 Hz, 2H, CH$_2$), 0.85 (t, J = 7.4 Hz, 3H, CH$_3$). ^{13}C NMR (DMSO-d$_6$): δ 154.9, 148.9, 147.7, 144.1, 136.3, 132.7, 130.5, 125.2, 124.6, 117.5, 41.3, 23.2, 11.7. HRMS (ESI) m/z found, 414.0117; C$_{15}$H$_{17}$BrN$_3$O$_4$S (M$^+$ + H) expected, 414.0123.

4.1.3.6 2-Iodopyridin-3-yl 4-(3-propylureido)benzenesulfonate (6). Flash chromatography (methylene chloride to methylene chloride/EtOAc (90 : 10)). Yield: 66%; white solid; mp: 165–167 °C. ^{1}H NMR (DMSO-d$_6$): δ 9.19 (s, 1H, NH), 8.34–8.32 (m, 1H, Ar), 7.75–7.68 (m, 4H, Ar), 7.61–7.47 (m, 2H, Ar), 6.45 (t, J = 5.7 Hz, 1H, NH), 3.07 (q, J = 6.6 Hz, 2H, CH$_2$), 1.47 (sext, J = 7.2 Hz, 2H, CH$_2$), 0.88 (t, J = 7.4 Hz, 3H, CH$_3$). ^{13}C NMR (DMSO-d$_6$): δ 154.9, 149.8, 147.7, 147.7, 130.6, 130.4, 124.9, 124.8, 117.6, 116.7, 41.4, 23.3, 11.8. HRMS (ESI) m/z found, 461.9976; C$_{15}$H$_{17}$IN$_3$O$_4$S (M$^+$ + H) expected, 461.9985.

4.1.3.7 2-Isopropylpyridin-3-yl 4-(3-propylureido) benzenesulfonate (7). Flash chromatography (methylene chloride to methylene chloride/EtOAc (90 : 10)). Yield: 52%; white solid; mp: 123–125 °C. ^{1}H NMR (DMSO-d$_6$): δ 9.13 (s, 1H, NH), 8.46–8.45 (m, 1H, Ar), 7.70–7.61 (m, 4H, Ar), 7.45–7.42 (m, 1H, Ar), 7.29–7.24 (m, 1H, Ar), 6.40 (t, J = 5.7 Hz, 1H, NH), 3.15–3.00 (m, 3H, CH and CH$_2$), 1.43 (sext, J = 7.0 Hz, 2H, CH$_2$), 0.97 (d, J = 6.7 Hz, 6H, 2 × CH$_3$), 0.85 (t, J = 7.4 Hz, 3H, CH$_3$). ^{13}C NMR (DMSO-d$_6$): δ 159.7, 154.9, 148.3, 147.4, 143.3, 130.4, 130.2, 125.1, 122.8, 117.6, 41.3, 28.8, 23.2, 21.9, 11.7. HRMS (ESI) m/z found, 378.1491; C$_{18}$H$_{24}$N$_3$O$_4$S (M$^+$ + H) expected, 378.1488.

4.1.3.8 2-Methylpyridin-3-yl 4-(3-propylureido) benzenesulfonate (8). Flash chromatography (methylene chloride to methylene chloride/EtOAc (90 : 10)). Yield: 68%; white solid; mp: 84–86 °C. ^{1}H NMR (DMSO-d$_6$): δ 9.14 (s, 1H, NH), 8.38–8.35 (m, 1H, Ar), 7.69–7.61 (m, 4H, Ar), 7.43–7.40 (m, 1H, Ar), 7.30–7.25 (m, 1H, Ar), 6.43–6.39 (m, 1H, NH), 3.04 (quint, J = 6.6 Hz, 2H, CH$_2$), 2.14 (s, 3H, CH$_3$), 1.43 (sext, J = 7.3 Hz, 2H, CH$_2$), 0.85 (t, J = 7.4 Hz, 3H, CH$_3$). ^{13}C NMR (DMSO-d$_6$): δ 154.9, 152.2, 148.0, 147.4, 144.7, 130.5, 130.2, 125.1, 123.1, 117.6, 41.3, 23.2, 19.5, 11.7. HRMS (ESI) m/z found, 350.1175; C$_{16}$H$_{20}$N$_3$O$_4$S (M$^+$ + H) expected, 350.1175.

4.1.3.9 2-Bromopyridin-3-yl 4-(3-(2-chloroethyl)ureido) benzenesulfonate (9). Flash chromatography (methylene chloride to methylene chloride/EtOAc (90 : 10)). Yield: 64%; white solid; mp: 135–137 °C. ^{1}H NMR (DMSO-d$_6$): δ 9.39 (s, 1H, NH), 8.34–8.32 (m, 1H, Ar), 7.74–7.63 (m, 5H, Ar), 7.54–7.49 (m, 1H, Ar), 6.66 (t, J = 5.9 Hz, 1H, NH), 3.66 (t, J = 6.0 Hz, 2H, CH$_2$), 3.46–3.40 (m, 2H, CH$_2$). ^{13}C NMR (DMSO-d$_6$): δ 154.8, 149.0, 147.4, 144.1, 136.3, 132.7, 130.6, 125.2, 125.0, 117.8, 44.6, 41.7. HRMS (ESI) m/z found, 433.9572; C$_{14}$H$_{14}$BrClN$_3$O$_4$S (M$^+$ + H) expected, 433.9577.

4.1.3.10 2-Iodopyridin-3-yl 4-(3-(2-chloroethyl)ureido) benzenesulfonate (10). Flash chromatography (methylene chloride to methylene chloride/EtOAc (90 : 10)). Yield: 52%; white solid; mp: 143–145 °C. ^{1}H NMR (DMSO-d$_6$): δ 9.39 (s, 1H, NH), 8.30–8.28 (m, 1H, Ar), 7.74–7.64 (m, 4H, Ar), 7.57–7.54 (m, 1H, Ar), 7.47–7.43 (m, 1H, Ar), 6.66 (t, J = 5.7 Hz, 1H, NH), 3.66 (t, J = 6.0 Hz, 2H, CH$_2$), 3.46–3.40 (m, 2H, CH$_2$). ^{13}C NMR (DMSO-d$_6$): δ 154.8, 149.8, 147.7, 147.4, 130.6, 130.4, 125.3, 124.8, 117.7, 116.6, 44.6, 41.7. HRMS (ESI) m/z found, 481.9426; C$_{14}$H$_{14}$ClIN$_3$O$_4$S (M$^+$ + H) expected, 481.9438.

4.1.3.11 2-Isopropylpyridin-3-yl 4-(3-(2-chloroethyl)ureido) benzenesulfonate (11). Flash chromatography (methylene chloride to methylene chloride/EtOAc (90 : 10)). Yield: 35%; white solid; mp: 127–129 °C. ^{1}H NMR (DMSO-d$_6$): δ 9.36 (s, 1H, NH), 8.47–8.45 (m, 1H, Ar), 7.68 (q, J = 9.0 Hz, 4H, Ar), 7.45–7.42 (m, 1H, Ar), 7.29–7.24 (m, 1H, Ar), 6.64 (t, J = 5.8 Hz, 1H, NH), 3.66 (t, J = 6.0 Hz, 2H, CH$_2$), 3.45–3.39 (m, 2H, CH$_2$), 3.11 (quint, J = 6.7 Hz, 1H, CH), 0.97 (d, J = 6.8 Hz, 6H, 2 × CH$_3$). ^{13}C NMR (DMSO-d$_6$): δ 159.7, 154.9, 148.3, 147.1, 143.3, 130.4, 130.2, 125.5, 122.9, 117.8, 44.6, 41.7, 28.8, 21.9. HRMS (ESI) m/z found, 398.0936; C$_{17}$H$_{21}$ClN$_3$O$_4$S (M$^+$ + H) expected, 398.0941.

4.1.3.12 4-Bromopyridin-3-yl 4-(3-ethylureido) benzenesulfonate (12). Flash chromatography (methylene

chloride to methylene chloride/EtOAc (90:10)). Yield: 13%; white solid; mp: 109–111 °C. ^{1}H NMR (DMSO-d_6): δ 9.20 (s, 1H, NH), 8.36–8.31 (m, 2H, Ar), 7.81–7.80 (m, 1H, Ar), 7.73–7.56 (m, 4H, Ar), 6.42–6.38 (m, 1H, NH), 3.10 (quint, J = 6.9 Hz, 2H, CH$_2$), 1.04 (t, J = 7.1 Hz, 3H, CH$_3$). ^{13}C NMR (DMSO-d_6): δ 154.8, 149.4, 147.8, 145.1, 144.4, 130.5, 129.4, 127.2, 124.5, 117.6, 34.5, 15.7. HRMS (ESI) m/z found 399.9967; C$_{14}$H$_{15}$BrN$_3$O$_4$S (M$^+$ + H) expected, 399.9967.

4.1.3.13 4-Iodopyridin-3-yl 4-(3-ethylureido)benzenesulfonate (13). Flash chromatography (methylene chloride to methylene chloride/EtOAc (90:10)). Yield: 60%; white solid; mp: 128–130 °C. ^{1}H NMR (DMSO-d_6): δ 9.18 (s, 1H, NH), 8.20 (s, 1H, Ar), 8.13–8.11 (m, 1H, Ar), 7.95–7.93 (m, 1H, Ar), 7.72–7.62 (m, 4H, Ar), 6.40–6.36 (m, 1H, NH), 3.10 (quint, J = 7.1 Hz, 2H, CH$_2$), 1.04 (t, J = 7.2 Hz, 3H, CH$_3$). ^{13}C NMR (DMSO-d_6): δ 154.8, 148.8, 147.9, 147.7, 143.6, 135.5, 130.6, 124.9, 117.6, 104.4, 34.5, 15.7. HRMS (ESI) m/z found, 447.9817; C$_{14}$H$_{15}$IN$_3$O$_4$S (M$^+$ + H) expected, 447.9828.

4.1.3.14 4-Methylpyridin-3-yl 4-(3-ethylureido) benzenesulfonate (14). Flash chromatography (methylene chloride to methylene chloride/EtOAc (90:10)). Yield: 70%; white solid; mp: 162–164 °C. ^{1}H NMR (DMSO-d_6): δ 9.17 (s, 1H, NH), 8.35–8.33 (m, 1H, Ar), 8.09–8.09 (m, 1H, Ar), 7.71–7.62 (m, 4H, Ar), 7.33–7.232 (m, 1H, Ar), 6.40–6.36 (m, 1H, NH), 3.11 (quint, J = 7.0 Hz, 2H, CH$_2$), 2.02 (s, 3H, CH$_3$), 1.04 (t, J = 7.2 Hz, 3H, CH$_3$). ^{13}C NMR (DMSO-d_6): δ 154.8, 148.3, 147.5, 145.6, 143.9, 141.1, 130.2, 127.0, 124.9, 117.6, 34.5, 15.7, 15.7. HRMS (ESI) m/z found, 336.1022; C$_{15}$H$_{18}$N$_3$O$_4$S (M$^+$ + H) expected, 336.1018.

4.1.3.15 4-Bromopyridin-3-yl 4-(3-propylureido) benzenesulfonate (15). Flash chromatography (methylene chloride to methylene chloride/EtOAc (90:10)). Yield: 23%; white solid; mp: 106–108 °C. ^{1}H NMR (DMSO-d_6): δ 9.17 (s, 1H, NH), 8.36–8.32 (m, 2H, Ar), 7.81–7.80 (m, 1H, Ar), 7.73–7.62 (m, 4H, Ar), 6.44–6.40 (m, 1H, NH), 3.08–3.01 (m, 2H, CH$_2$), 1.44 (sext, J = 7.2 Hz, 2H, CH$_2$), 0.85 (t, J = 7.4 Hz, 3H, CH$_3$). ^{13}C NMR (DMSO-d_6): δ 154.9, 149.4, 147.8, 145.1, 144.4, 130.6, 129.4, 127.2, 124.5, 117.6, 41.3, 23.2, 11.7. HRMS (ESI) m/z found, 414.0114; C$_{15}$H$_{17}$BrN$_3$O$_4$S (M$^+$ + H) expected, 414.0123.

4.1.3.16 4-Iodopyridin-3-yl 4-(3-propylureido) benzenesulfonate (16). Flash chromatography (methylene chloride to methylene chloride/EtOAc (90:10)). Yield: 70%; white solid; mp: 125–127 °C. ^{1}H NMR (DMSO-d_6): δ 9.16 (s, 1H, NH), 8.20 (s, 1H, Ar), 8.13–8.10 (m, 1H, Ar), 7.95–7.93 (m, 1H, Ar), 7.72–7.62 (m, 4H, Ar), 6.41 (t, J = 5.7 Hz, 1H, NH), 3.04 (q, J = 6.3 Hz, 2H, CH$_2$), 1.43 (sext, J = 7.2 Hz, 2H, CH$_2$), 0.85 (t, J = 7.4 Hz, 3H, CH$_3$). ^{13}C NMR (DMSO-d_6): δ 154.9, 148.8, 147.9, 147.7, 143.5, 135.5, 130.6, 124.9, 117.6, 104.4, 41.3, 23.2, 11.7. HRMS (ESI) m/z found, 461.9979; C$_{15}$H$_{17}$IN$_3$O$_4$S (M$^+$ + H) expected, 461.9985.

4.1.3.17 4-Methylpyridin-3-yl 4-(3-propylureido) benzenesulfonate (17). Flash chromatography (methylene chloride to methylene chloride/EtOAc (90:10)). Yield: 67%; white solid; mp: 113–115 °C. ^{1}H NMR (DMSO-d_6): δ 9.16 (s, 1H, NH), 8.35–8.33 (m, 1H, Ar), 8.09 (s, 1H, Ar), 7.71–7.62 (m, 4H, Ar), 7.34–7.32 (m, 1H, Ar), 6.42 (t, J = 5.7 Hz, 1H, NH), 3.04 (q, J = 6.3 Hz, 2H, CH$_2$), 2.02 (s, 3H, CH$_3$), 1.43 (sext, J = 7.3 Hz, 2H, CH$_2$), 0.85 (t, J = 7.4 Hz, 3H, CH$_3$). ^{13}C NMR (DMSO-d_6): δ 154.9, 148.3, 147.5, 145.6, 143.8, 141.1, 130.2, 127.0, 124.9, 117.6, 41.3, 23.2, 15.7, 11.7. HRMS (ESI) m/z found, 350.1172; C$_{16}$H$_{20}$N$_3$O$_4$S (M$^+$ + H) expected, 350.1175.

4.1.3.18 4-Iodopyridin-3-yl 4-(3-(2-chloroethyl)ureido) benzenesulfonate (18). Flash chromatography (methylene chloride to methylene chloride/EtOAc (90:10)). Yield: 50%; white solid; mp: 126–128 °C. ^{1}H NMR (DMSO-d_6): δ 9.40 (s, 1H, NH), 8.21 (s, 1H, Ar), 8.13–8.11 (m, 1H, Ar), 7.95–7.93 (m, 1H, Ar), 7.74–7.64 (m, 4H, Ar), 6.68–6.64 (m, 1H, NH), 3.66 (t, J = 6.1 Hz, 2H, CH$_2$), 3.43 (q, J = 6.0 Hz, 2H, CH$_2$). ^{13}C NMR (DMSO-d_6): δ 154.9, 148.8, 147.9, 147.4, 143.6, 135.5, 130.6, 125.3, 117.8, 104.4, 44.6, 41.7. HRMS (ESI) m/z found, 481.9431; C$_{14}$H$_{14}$ClIN$_3$O$_4$S (M$^+$ + H) expected, 481.9438.

4.1.4 General preparation of PYRUB-SO salts 19–36. The selected PYRUB-SO (0.4 mmol, 1.0 eq.) was dissolved to a solution of tetrahydrofuran (THF) and stirred at room temperature. Hydrogen chloride (HCl in diethyl ether 1 M, 1.2 mmol, 3.0 eq.) was added to the reaction mixture, which was stirred for 16 h. The resulting precipitate was filtered off and triturated in a cold mixture of hexanes and subsequently diethyl ether. Finally, the solid was collected and dried under vacuum to afford the desired PYRUB-SO hydrochloride salt.

4.1.5 Characterization of PYRUB-SOs salts 19–36

4.1.5.1 2-Bromopyridin-3-yl 4-(3-ethylureido)benzenesulfonate hydrochloride (19). Yield: 90%; light brown solid; mp: decomposes at 80 °C. ^{1}H NMR (DMSO-d_6): δ 9.20 (s, 1H, NH), 8.37–8.32 (m, 1H, Ar), 7.77–7.63 (m, 5H, Ar), 7.55–7.49 (m, 1H, Ar), 6.40 (brs, 1H, NH), 3.85 (brs, 2H, CH$_2$), 1.06 (t, J = 7.2 Hz, 3H, CH$_3$). ^{13}C NMR (DMSO-d_6): δ 154.3, 148.5, 147.9, 147.3, 133.0, 132.2, 130.0, 124.6, 124.1, 117.1, 34.0, 15.2. HRMS (ESI) m/z found, 399.9962; C$_{14}$H$_{15}$BrN$_3$O$_4$S (M$^+$ + H) expected, 399.9967.

4.1.5.2 2-Iodopyridin-3-yl 4-(3-ethylureido)benzenesulfonate hydrochloride (20). Yield: 75%; yellowish solid; mp: decomposes at 115 °C. ^{1}H NMR (DMSO-d_6): δ 9.30 (s, 1H, NH), 8.32–8.30 (m, 1H, Ar), 7.69 (q, J = 8.8 Hz, 4H, Ar), 7.58–7.56 (m, 1H, Ar), 7.49–7.45 (m, 1H, Ar), 6.46 (brs, 1H, NH), 4.16 (brs, 1H, NH), 3.12–3.12 (m, 2H, CH$_2$), 1.06 (t, J = 7.1 Hz, 3H, CH$_3$). ^{13}C NMR (DMSO-d_6): δ 154.4, 149.3, 148.0, 147.3, 147.3, 130.2, 130.0, 124.4, 117.1, 116.2, 34.1, 15.3. HRMS (ESI) m/z found, 447.9820; C$_{14}$H$_{15}$IN$_3$O$_4$S (M$^+$ + H) expected, 447.9828.

4.1.5.3 2-Isopropylpyridin-3-yl 4-(3-ethylureido) benzenesulfonate hydrochloride (21). Yield: 96%; white solid; mp: decomposes at 132 °C. ^{1}H NMR (DMSO-d_6): δ 9.67 (s, 1H, NH), 8.53–8.51 (m, 1H, Ar), 7.72–7.64 (m, 5H, Ar and NH), 7.60–7.57 (m, 1H, Ar), 7.42–7.38 (m, 1H, Ar), 6.68 (brs, 1H, NH), 3.20–3.08 (m, 3H, CH and CH$_2$), 1.10–1.01 (m, 9H, 3 × CH$_3$). ^{13}C NMR (DMSO-d_6): δ 158.7, 154.5, 147.3, 146.7, 143.2, 131.7, 129.8, 124.1, 123.1, 117.0, 34.0, 28.2, 21.3, 15.2. HRMS (ESI) m/z found, 364.1327; C$_{17}$H$_{22}$N$_3$O$_4$S (M$^+$ + H) expected, 364.1331.

4.1.5.4 2-Methylpyridin-3-yl 4-(3-ethylureido)benzenesulfonate hydrochloride (22). Yield: 96%; off-white solid; mp: decomposes

at 152 °C. ^{1}H NMR (DMSO-d$_6$): δ 9.74 (s, 1H, NH), 8.55–8.53 (m, 1H, Ar), 7.77–7.65 (m, 5H, Ar), 7.59–7.54 (m, 1H, Ar), 6.70 (brs, 1H, NH), 5.60 (brs, 1H, NH), 3.12 (q, J = 7.2 Hz, 2H, CH$_2$), 2.26 (s, 3H, CH$_3$), 1.05 (t, J = 7.2 Hz, 3H, CH$_3$). ^{13}C NMR (DMSO-d$_6$): δ 154.5, 150.7, 147.5, 144.9, 144.7, 133.8, 129.9, 124.0, 123.9, 117.1, 34.0, 17.4, 15.3. HRMS (ESI) m/z found, 336.1018; C$_{15}$H$_{18}$N$_3$O$_4$S (M$^+$ + H) expected, 336.1018.

4.1.5.5 2-Bromopyridin-3-yl 4-(3-propylureido) benzenesulfonate hydrochloride (23). Yield: 96%; white solid; mp: decomposes at 156 °C. ^{1}H NMR (DMSO-d$_6$): δ 9.19 (s, 1H, NH), 8.38–8.34 (m, 1H, Ar), 7.77–7.63 (m, 5H, Ar), 7.56–7.51 (m, 1H, Ar), 6.44 (t, J = 5.6 Hz, 1H, NH), 3.06 (q, J = 6.6 Hz, 2H, CH$_2$), 1.45 (sext, J = 7.3 Hz, 2H, CH$_2$), 0.87 (t, J = 7.4 Hz, 3H, CH$_3$). ^{13}C NMR (DMSO-d$_6$): δ 154.4, 148.5, 147.3, 143.7, 135.9, 132.3, 130.1, 124.8, 124.2, 117.1, 40.9, 22.8, 11.3. HRMS (ESI) m/z found, 414.0116; C$_{15}$H$_{17}$BrN$_3$O$_4$S (M$^+$ + H) expected, 414.0123.

4.1.5.6 2-Iodopyridin-3-yl 4-(3-propylureido)benzenesulfonate hydrochloride (24). Yield: 73%; white solid; mp: decomposes at 133 °C. ^{1}H NMR (DMSO-d$_6$): δ 9.19 (m, 1H, NH), 8.32–8.30 (m, 1H, Ar), 7.73–7.56 (m, 6H, Ar and NH), 7.49–7.45 (m, 1H, Ar), 6.44 (t, J = 5.7 Hz, 1H, NH), 3.40 (s, 1H, NH), 3.06 (q, J = 6.9 Hz, 2H, CH$_2$), 1.45 (sext, J = 7.3 Hz, 2H, CH$_2$), 0.87 (t, J = 7.4 Hz, 3H, CH$_3$). ^{13}C NMR (DMSO-d$_6$): δ 154.4, 149.3, 147.3, 143.6, 130.2, 130.0, 124.4, 124.4, 117.1, 116.2, 40.9, 22.8, 11.3. HRMS (ESI) m/z found, 461.9981; C$_{15}$H$_{17}$IN$_3$O$_4$S (M$^+$ + H) expected, 461.9985.

4.1.5.7 2-Isopropylpyridin-3-yl 4-(3-propylureido) benzenesulfonate hydrochloride (25). Yield: 98%; white solid; mp: decomposes at 157 °C. ^{1}H NMR (DMSO-d$_6$): δ 9.60 (s, 1H, NH), 8.51–8.49 (m, 1H, Ar), 7.72–7.52 (m, 5H, Ar), 7.38–7.34 (m, 1H, Ar), 6.67 (brs, 1H, NH), 5.19 (brs, 1H, NH), 3.19–3.03 (m, 3H, CH and CH$_2$), 1.44 (h, J = 7.3 Hz, 2H, CH$_2$), 1.01 (d, J = 6.8 Hz, 6H, 2 × CH$_3$), 0.87 (t, J = 7.4 Hz, 3H, CH$_3$). ^{13}C NMR (DMSO-d$_6$): δ 158.9, 154.6, 147.2, 147.2, 143.1, 131.1, 129.8, 124.3, 122.9, 117.1, 40.8, 28.2, 22.8, 21.4, 11.3. HRMS (ESI) m/z found, 378.1486; C$_{18}$H$_{24}$N$_3$O$_4$S (M$^+$ + H) expected, 378.1488.

4.1.5.8 2-Methylpyridin-3-yl 4-(3-propylureido) benzenesulfonate hydrochloride (26). Yield: 98%; white solid; mp: decomposes at 120 °C. ^{1}H NMR (DMSO-d$_6$): δ 9.81 (s, 1H, NH), 8.58–8.54 (m, 1H, Ar), 7.80–7.56 (m, 6H, Ar), 6.79 (brs, 1H, NH), 5.20 (brs, 1H, NH), 3.08–3.03 (m, 2H, CH$_2$), 2.28–2.16 (m, 3H, CH$_3$), 1.48–1.39 (m, 2H, CH$_2$), 0.88 (t, J = 7.4 Hz, 3H, CH$_3$). ^{13}C NMR (DMSO-d$_6$): δ 154.7, 150.6, 147.5, 145.0, 144.4, 134.2, 130.0, 124.2, 123.8, 117.1, 40.8, 22.8, 17.2, 11.4. HRMS (ESI) m/z found, 350.1174; C$_{16}$H$_{20}$N$_3$O$_4$S (M$^+$ + H) expected, 350.1175.

4.1.5.9 2-Bromopyridin-3-yl 4-(3-(2-chloroethyl)ureido) benzenesulfonate hydrochloride (27). Yield: 89%; white solid; mp: decomposes at 97 °C. ^{1}H NMR (DMSO-d$_6$): δ 9.42 (s, 1H, NH), 8.38–8.34 (m, 1H, Ar), 7.77–7.65 (m, 5H, Ar), 7.56–7.51 (m, 1H, Ar), 6.68 (t, J = 5.8 Hz, 1H, NH), 3.67 (t, J = 6.0 Hz, 2H, CH$_2$), 3.47–3.45 (m, 2H, CH$_2$ and NH). ^{13}C NMR (DMSO-d$_6$): δ 154.4, 148.5, 148.0, 147.0, 143.7, 133.1, 132.3, 130.1, 124.8, 117.3, 44.1, 41.2. HRMS (ESI) m/z found, 433.9570; C$_{14}$H$_{14}$BrClN$_3$O$_4$S (M$^+$ + H) expected, 433.9577.

4.1.5.10 2-Iodopyridin-3-yl 4-(3-(2-chloroethyl)ureido) benzenesulfonate hydrochloride (28). Yield: 87%; dark yellow solid; mp: decomposes at 92 °C. ^{1}H NMR (DMSO-d$_6$): δ 9.42 (s, 1H, NH), 8.38–8.30 (m, 1H, Ar), 7.77–7.64 (m, 4H, Ar), 7.59–7.45 (m, 2H, Ar), 6.68 (t, J = 5.7 Hz, 1H, NH), 3.67 (t, J = 6.1 Hz, 2H, CH$_2$), 3.60 (s, 1H, NH), 3.44 (q, J = 6.0 Hz, 2H, CH$_2$). ^{13}C NMR (DMSO-d$_6$): δ 154.4, 149.3, 147.3, 146.9, 130.2, 130.0, 124.8, 124.4, 117.3, 116.2, 44.1, 41.2. HRMS (ESI) m/z found, 481.9425; C$_{14}$H$_{14}$ClIN$_3$O$_4$S (M$^+$ + H) expected, 481.9438.

4.1.5.11 2-Isopropylpyridin-3-yl 4-(3-(2-chloroethyl)ureido) benzenesulfonate hydrochloride (29). Yield: 94%; white solid; mp: decomposes at 163 °C. ^{1}H NMR (DMSO-d$_6$): δ 9.79 (s, 1H, NH), 8.52–8.50 (m, 1H, Ar), 7.74–7.66 (m, 4H, Ar), 7.55–7.53 (m, 1H, Ar), 7.39–7.34 (m, 1H, Ar), 6.88 (brs, 1H, NH), 5.99 (brs, 1H, NH), 3.66 (t, J = 5.9 Hz, 2H, CH$_2$), 3.46–3.41 (m, 2H, CH$_2$), 3.15 (p, J = 6.7 Hz, 1H, CH), 1.01 (d, J = 6.8 Hz, 6H, 2 × CH$_3$). ^{13}C NMR (DMSO-d$_6$): δ 158.9, 154.6, 147.2, 146.9, 143.1, 131.1, 129.9, 124.7, 122.9, 117.3, 44.1, 41.2, 28.2, 21.4. HRMS (ESI) m/z found, 398.0938; C$_{17}$H$_{21}$ClN$_3$O$_4$S (M$^+$ + H) expected, 398.0941.

4.1.5.12 4-Bromopyridin-3-yl 4-(3-ethylureido) benzenesulfonate hydrochloride (30). Yield: 98%; white solid; mp: decomposes at 109 °C. ^{1}H NMR (DMSO-d$_6$): δ 9.25 (s, 1H, NH), 8.81 (s, 1H, Ar), 8.59 (d, J = 5.4 Hz, 1H, Ar), 7.79–7.74 (m, 2H, Ar), 7.68–7.64 (m, 2H, Ar), 7.37 (d, J = 5.4 Hz, 1H, Ar), 6.43 (t, J = 5.6 Hz, 1H, NH), 3.16–3.05 (m, 2H, CH$_2$), 1.05 (t, J = 7.1 Hz, 3H, CH$_3$). ^{13}C NMR (DMSO-d$_6$): δ 154.8, 154.0, 153.3, 151.2, 147.9, 130.5, 124.5, 118.8, 117.6, 114.5, 34.5, 15.7. HRMS (ESI) m/z found 399.9962; C$_{14}$H$_{15}$BrN$_3$O$_4$S (M$^+$ + H) expected, 399.9967.

4.1.5.13 4-Iodopyridin-3-yl 4-(3-ethylureido)benzenesulfonate hydrochloride (31). Yield: 79%; off-white solid; mp: decomposes at 142 °C. ^{1}H NMR (DMSO-d$_6$): δ 9.66 (s, 1H, NH), 8.44 (brs, 1H, NH), 8.26 (s, 1H, Ar), 8.15 (d, J = 5.1 Hz, 1H, Ar), 7.99 (d, J = 5.1 Hz, 1H, Ar), 7.73–7.65 (m, 4H, Ar), 6.67 (brs, 1H, NH), 3.12 (q, J = 7.2 Hz, 2H, CH$_2$), 1.05 (t, J = 7.2 Hz, 3H, CH$_3$). ^{13}C NMR (DMSO-d$_6$): δ 154.5, 147.9, 147.6, 147.4, 142.7, 135.2, 130.2, 124.2, 117.0, 104.9, 34.0, 15.3. HRMS (ESI) m/z found, 447.9820; C$_{14}$H$_{15}$IN$_3$O$_4$S (M$^+$ + H) expected, 447.9828.

4.1.5.14 4-Methylpyridin-3-yl 4-(3-ethylureido) benzenesulfonate hydrochloride (32). Yield: 98%; white solid; mp: decomposes at 173 °C. ^{1}H NMR (DMSO-d$_6$): δ 9.88 (s, 1H, NH), 8.58–8.56 (m, 1H, Ar), 8.46 (s, 1H, Ar), 7.99 (s, 1H, NH), 7.75–7.65 (m, 5H, Ar), 6.80 (brs, 1H, NH), 3.11 (q, J = 7.4 Hz, 2H, CH$_2$), 2.08 (s, 3H, CH$_3$), 1.05 (t, J = 7.2 Hz, 3H, CH$_3$). ^{13}C NMR (DMSO-d$_6$): δ 154.6, 147.6, 146.8, 145.6, 144.0, 140.1, 130.0, 128.2, 123.6, 117.1, 34.0, 15.8, 15.3. HRMS (ESI) m/z found, 336.1016; C$_{15}$H$_{18}$N$_3$O$_4$S (M$^+$ + H) expected, 336.1018.

4.1.5.15 4-Bromopyridin-3-yl 4-(3-propylureido) benzenesulfonate hydrochloride (33). Yield: 96%; white solid; mp: decomposes at 115 °C. ^{1}H NMR (DMSO-d$_6$): δ 9.59 (s, 1H, NH), 8.50–8.35 (m, 2H, Ar), 7.84 (d, J = 5.2 Hz, 1H, Ar), 7.74–7.58 (m, 4H, Ar), 6.67 (s, 1H, NH), 6.28 (brs, 1H, NH), 3.11–3.00 (m, 2H, CH$_2$), 1.44 (h, J = 7.3 Hz, 2H, CH$_2$), 0.87 (t,

J = 7.4 Hz, 3H, CH$_3$). ^{13}C NMR (DMSO-d$_6$): δ 154.6, 148.8, 147.4, 144.5, 144.0, 130.2, 129.1, 127.0, 123.9, 117.0, 40.9, 22.8, 11.3. HRMS (ESI) m/z found, 414.0119; C$_{15}$H$_{17}$BrN$_3$O$_4$S (M$^+$ + H) expected, 414.0123.

4.1.5.16 4-Iodopyridin-3-yl 4-(3-propylureido) benzenesulfonate hydrochloride (34). Yield: 91%; off-white solid; mp: decomposes at 133 °C. ^{1}H NMR (DMSO-d$_6$): δ 9.72 (s, 1H, NH), 8.27 (s, 1H, Ar), 8.16 (d, J = 5.1 Hz, 1H, Ar), 8.00 (d, J = 5.1 Hz, 1H, Ar), 7.72–7.64 (m, 4H, Ar), 7.07 (brs, 1H, NH), 6.78 (brs, 1H, NH), 3.05 (t, J = 7.0 Hz, 2H, CH$_2$), 1.44 (h, J = 7.3 Hz, 2H, CH$_2$), 0.87 (t, J = 7.4 Hz, 3H, CH$_3$). ^{13}C NMR (DMSO-d$_6$): δ 154.7, 147.7, 147.7, 147.5, 142.6, 135.3, 130.2, 124.2, 117.0, 105.2, 40.8, 22.8, 11.4. HRMS (ESI) m/z found, 461.9976; C$_{15}$H$_{17}$IN$_3$O$_4$S (M$^+$ + H) expected, 461.9985.

4.1.5.17 4-Methylpyridin-3-yl 4-(3-propylureido) benzenesulfonate hydrochloride (35). Yield: 96%; white solid; mp: decomposes at 156 °C. ^{1}H NMR (DMSO-d$_6$): δ 9.90 (s, 1H, NH), 8.59–8.56 (m, 1H, Ar), 8.46–8.45 (m, 1H, Ar), 7.75–7.65 (m, 5H, Ar), 6.83 (s, 1H, NH), 6.42 (brs, 1H, NH), 3.08–3.02 (m, 2H, CH$_2$), 2.09–2.08 (m, 3H, CH$_3$), 1.50–1.38 (m, 2H, CH$_2$), 0.87 (t, J = 7.4 Hz, 3H, CH$_3$). ^{13}C NMR (DMSO-d$_6$): δ 155.1, 148.0, 147.1, 146.0, 144.5, 140.6, 130.4, 128.5, 124.0, 117.4, 41.2, 23.2, 16.2, 11.8. HRMS (ESI) m/z found, 350.1173; C$_{16}$H$_{20}$N$_3$O$_4$S (M$^+$ + H) expected, 350.1175.

4.1.5.18 4-Iodopyridin-3-yl 4-(3-(2-chloroethyl)ureido) benzenesulfonate hydrochloride (36). Yield: 98%; white solid; mp: decomposes at 93 °C. ^{1}H NMR (DMSO-d$_6$): δ 9.80 (s, 1H, NH), 8.24 (s, 1H, Ar), 8.24–8.12 (m, 1H, Ar), 7.98–7.96 (m, 1H, Ar), 7.73–7.65 (m, 4H, Ar), 6.88 (s, 1H, NH), 5.62 (brs, 1H, NH), 3.65 (t, J = 6.1 Hz, 2H, CH$_2$), 3.43–3.41 (m, 2H, CH$_2$). ^{13}C NMR (DMSO-d$_6$): δ 155.0, 148.3, 148.0, 147.5, 143.2, 135.6, 130.6, 125.1, 117.7, 105.2, 44.5, 41.6. HRMS (ESI) m/z found, 481.9427; C$_{14}$H$_{14}$ClIN$_3$O$_4$S (M$^+$ + H) expected, 481.9438.

4.1.6 General preparation of compounds 37–39. The synthesis of alkylphenylureas **37** and **38** is based on the modification of a protocol for the preparation of compound **39** published by Fortin *et al.*[47,48] Briefly, the required isocyanate (16.5 mmol, 1.1 eq.) was slowly added to a solution of aniline (15.0 mmol, 1.0 eq.) in diethyl ether (50 mL) at 0 °C. The reaction mixture was stirred for 16 h at room temperature, and the resulting precipitate was filtered and successively washed with diethyl ether and a cold mixture of diethyl ether and hexanes. The product was dried under vacuum and used without further purification.

4.1.7 Characterization of compounds 37 and 38

4.1.7.1 1-Ethyl-3-phenylurea (37). Yield: 85%; white solid; mp: 99–101 °C. ^{1}H NMR (CDCl$_3$): δ 7.64 (s, 1H, NH), 7.32–7.16 (m, 4H, Ar), 7.05–6.93 (m, 1H, Ar), 5.66 (s, 1H, NH), 3.20 (q, J = 6.6 Hz, 2H, CH$_2$), 1.06 (t, J = 7.2 Hz, 3H, CH$_3$). ^{13}C NMR (CDCl$_3$): δ 156.7, 139.0, 129.0, 123.0, 120.3, 34.9, 15.3.

4.1.7.2 1-Phenyl-3-propylurea (38). Yield: 77%; white solid; mp: 116–118 °C. ^{1}H NMR (CDCl$_3$): δ 7.59 (s, 1H, NH), 7.32–7.16 (m, 4H, Ar), 7.05–6.93 (m, 1H, Ar), 5.70 (s, 1H, NH), 3.12 (t, J = 7.3 Hz, 2H, CH$_2$), 1.45 (sext, J = 7.4 Hz, 2H, CH$_2$), 0.85 (t, J = 7.5 Hz, 3H, CH$_3$). ^{13}C NMR (CDCl$_3$): δ 156.8, 139.0, 129.0, 123.1, 120.3, 41.9, 23.3, 11.3.

4.1.8 General preparation of compounds 40–42. The synthesis of compounds **40** and **41** is based on the modification of a protocol for the preparation of compound **42** published by Gagné-Boulet *et al.*[24] Briefly, the alkylphenylurea **37**, **38** or **39** (10 mmol, 1.0 eq.) was slowly added to a solution of chlorosulfonic acid (80 mmol, 8.0 eq.) at 0 °C. The chlorosulfonic acid solution of compounds **40** and **41** was first stirred for 30 min at 0 °C and then for an additional hour at 60 °C. For compound **42**, the mixture was first stirred at 0 °C for 30 min and then at room temperature for 16 h. Then, the reaction mixture was poured slowly into ice water to quench the acid in excess. The resulting precipitate was filtered, rinsed with water, and dried under vacuum overnight. The product was purified by flash chromatography.

4.1.9 Characterization of compounds 40 and 41

4.1.9.1 4-(3-Ethylureido)benzenesulfonyl chloride (40). Flash chromatography (hexanes to hexanes/EtOAc (60 : 40)). Yield: 56%; white solid; mp: 143–145 °C. ^{1}H NMR (DMSO-d$_6$): δ 8.82 (s, 1H, NH), 7.52–7.30 (m, 5H, Ar and NH), 3.06 (q, J = 7.2 Hz, 2H, CH$_2$), 1.01 (t, J = 7.2 Hz, 3H, CH$_3$). ^{13}C NMR (DMSO-d$_6$): δ 155.5, 141.9, 139.9, 126.6, 116.7, 34.3, 15.8.

4.1.9.2 4-(3-Propylureido)benzenesulfonyl chloride (41). Flash chromatography (hexanes to hexanes/EtOAc (60 : 40)). Yield: 70%; white solid; mp: 133–135 °C. ^{1}H NMR (DMSO-d$_6$): δ 9.75 (s, 1H, NH), 8.76 (s, 1H, NH), 7.51–7.26 (m, 4H, Ar), 3.00 (t, J = 7.0 Hz, 2H, CH$_2$), 1.40 (sext, J = 7.3 Hz, 2H, CH$_2$), 0.84 (t, J = 7.4 Hz, 3H, CH$_3$). ^{13}C NMR (DMSO-d$_6$): δ 155.6, 141.8, 140.1, 126.6, 116.7, 41.2, 23.4, 11.8.

4.1.10 Water solubility evaluation. The water solubility of PYRUB-SOs **1–36** and PUB-SOs (SFOM-0106, SFOM-0107, SFOM-0111, SFOM-0147, SFOM-0148 and SFOM-0149) was assessed using the shake-flask method in ultrapure water.[49–51] Initially, a standard calibration curve for each drug was obtained *via* UV spectroscopy using a SpectraMax® i3x spectrometer (Molecular Devices, San Jose, CA, USA) from a DMSO stock solution diluted in an 80/20 water/acetonitrile mixture (v/v). Afterwards, an aliquot of the stock solution for each compound in DMSO was added to ultrapure water (final DMSO concentration of 1% (v/v)). The mixture underwent sonication for 10 min and then shaken at 130 rpm for 24 h at 37 °C. The resulting suspension was centrifuged for 5 min at 5000 rpm, and the supernatant collected and diluted with acetonitrile to form an 80/20 water/acetonitrile solution (v/v). This solution was analyzed by UV absorbance using a SpectraMax® i3x spectrometer at the appropriate wavelength (270 to 290 nm). The concentration of the solubilized compound in the supernatant was determined using the standard calibration curve. Compound solutions were prepared in triplicate, and each sample was analyzed thrice. Errors are reported as SEM.

4.2 Biological methods

4.2.1 Cell culture. MCF7 human breast carcinoma, HT-29 human colon carcinoma, HT-1080 human fibrosarcoma, THP-1 acute monocytic leukemia and HL-60 acute promyelocytic leukemia cells were bought from the

American Type Culture Collection (ATCC, Manassas, VA, USA). M21 human melanoma cells were kindly provided by Dr. David Cheresh (University of California, San Diego School of Medicine, CA, USA). MOLM-13 acute monocytic leukemia cells were purchased from Leibniz Institute DSMZ (Braunschweig, Lower Saxony, Germany). MCF7 cells were cultured in Eagle's minimum essential medium (EMEM, ATCC) supplemented with 0.01 mg mL^{-1} recombinant human insulin (Gibco, Thermo Fisher Scientific, Saint-Laurent, QC, Canada) and 10% (v/v) fetal bovine serum (FBS, Gibco). HT-29, M21 and HT-1080 were maintained in Dulbecco's modified Eagle medium (DMEM, Gibco) supplemental with 10% (v/v) of FBS for HT-29 and 5% (v/v) for remaining cells. THP-1 and MOLM-13 cells were cultured in RPMI-1640 medium (Wisent Bioproducts, St-Bruno, QC, Canada) supplemented with 10% (v/v) of FBS. HL-60 cells were maintained in Iscove's modified Dulbecco's medium (IMDM, Wisent Bioproducts) supplemented with 20% (v/v) of FBS. All mediums were supplemented with 1% (v/v) penicillin–streptomycin (Wisent Bioproducts). The cells were cultured at 37 °C in moisture saturated atmosphere containing 5% CO_2.

4.2.2 Antiproliferative activity assay

4.2.2.1 SRB assay. The antiproliferative activity of PYRUB-SOs 4.1–4.36, SFOM-0046 and brequinar was assessed using a modified protocol of the National Cancer Institute (NCI) drug screening program.[39] Briefly, 96-well plates (Corning Costar®, Thermo Fisher Scientific, Saint-Laurent, QC, Canada) were seeded with either MCF7 (3.5×10^3 cells per well), HT-29 (3.5×10^3 cells per well), M21 (3×10^3 cells per well) or HT-1080 (3×10^3 cells per well) cells suspended (75 μL) in an appropriate culture medium and incubated for 24 h at 37 °C as described in section 4.2.1. Subsequently, freshly solubilized drugs in DMSO were serially diluted and added (75 μL) to the plates, maintaining DMSO concentration constant at 0.5% (v/v). Cells were treated with the drugs for 48 h, and then the treatment was stopped by discarding the culture medium and adding a cold trichloroacetic acid (10%, w/v) solution to the plates, which were kept at 4 °C for 2 h. Afterwards, the acid solution was discarded, and the plates were washed 4 times with distilled water and air-dried at room temperature. Cells were then stained with sulforhodamine B (SRB, Thermo Fisher Scientific, Saint-Laurent, QC, Canada) solution (0.1% w/v in 1% acetic acid) for 30 min. After washing the cells 4 times with a solution of 1% (v/v) acetic acid, 200 μL of Tris base 20 mM (Bio Basic, Markham, ON, Canada) was added to dissolve the cell-bound dye and the absorbance was evaluated at a wavelength between 520 and 580 nm using a SpectraMax® i3x spectrophotometer (Molecular Devices). Finally, the absorbance from both treated and sham-treated cells (fixed on the treatment day) was compared to determine each drug's cell growth inhibition percentage. IC$_{50}$ values and SEM were calculated using GraphPad Prism 10.1.2 software (GraphPad Software, San Jose, CA, USA). Each experiment was repeated three times in triplicate.

4.2.2.2 MTT assay. The antiproliferative activity of PYRUB-SOs 4.1–4.36, SFOM-0046 and brequinar on AML MOLM-13, THP-1 and HL-60 cell lines was carried out using the MTT colorimetric assay based on the protocol published by the ATCC with slight modifications.[40] Briefly, AML cells were seeded in 96 well plates at a density of 2.5×10^4 cells per well for THP-1 and 2.0×10^4 cells per well for both MOLM-13 and HL-60 cell lines and they were incubated at 37 °C for 24 h, as described in section 4.2.1. Afterwards, drugs freshly solubilized in DMSO were serially diluted in the appropriate medium, and 75 μL of the solution was added to the wells, which were reincubated for 48 h. The final concentration of DMSO in the culture media was kept at 0.5% (v/v) in all experiments. After the treatment period, 10 μL of MTT (5 mg mL^{-1} in PBS) was added to the wells that were kept in the incubator for 6 h. Afterward, the cells were solubilized by adding 100 μL of 10% (w/v) sodium dodecyl sulfate (SDS) in 0.01 M HCl, and the plates were reincubated in the dark for 16 h. The optical density was read at 595 nm using a SpectraMax® i3x (Molecular Devices). The absorbance from treated cells was compared to sham-treated cell plates that were fixed on the day of treatment. The percentage of cell viability for each drug was calculated using GraphPad Prism version 10.1.2 (GraphPad Software). The experiments were done thrice in triplicate.

4.2.3 Cell cycle arrest analysis. M21, MOLM-13 and THP-1 cells were seeded into 6-well plates (Corning Costar®, Thermo Fisher Scientific, Saint-Laurent, QC, Canada) at a density of 3.5×10^5 cells per well and cultured at 37 °C for 24 h, as described in section 4.2.1. Subsequently, the cells were treated with selected PYRUB-SOs, SFOM-0046 or brequinar for 24 h at 2- and 5-fold their respective IC$_{50}$. SFOM-0046 and brequinar were positive controls, while DMSO (0.25% (v/v) for MOL-13 and THP-1 cells and 0.5% (v/v) for M21 cells) was the excipient. Following the treatments, non-adherent AML cells were transferred directly into 5 mL culture tubes (Sarstedt, Nümbrecht, Germany) while the M21 adherent cells were detached using trypsin (Wisent Bioproducts) and transferred into 5 mL culture tubes. Thereafter, the cells were centrifuged, washed with phosphate-buffered saline (PBS, Life Technologies, Thermo Fisher Scientific, Saint-Laurent, QC, Canada), and fixed with 750 μL of cold ethanol while vortexing, then stored at −20 °C until analysis. Before flow cytometry, the cells were washed with PBS and resuspended in 350 μL of PBS containing 2 μg mL^{-1} of 4′,6′-diamidino-2-phenylindole (DAPI, MilliporeSigma, St. Louis, MO, USA). Cell cycle distribution was analyzed using an LSR II flow cytometer (BD Biosciences, Franklin Lakes, NJ, USA) and processed with FlowJo 10.8 software (BD Biosciences, Franklin Lakes, NJ, USA). Each experiment was conducted in triplicate, and errors are presented as SEM.

4.2.4 H2AX phosphorylation. The experiments were conducted using the procedure reported by Gagné-Boulet *et al.*[25] Briefly, M21 cells were seeded in 24-well plates (1.5×10^4 cells per well) on fibronectin-coated glass coverslips (12 mm) and incubated at 37 °C for 24 h. Subsequently, the cells

were treated with PYRUB-SOs **2**, **3**, **20** or **21** at 2-fold their respective IC_{50} for 24 h. SFOM-0046 and brequinar served as positive controls, while 0.5% DMSO served as excipient. After treatment, the cells were washed with PBS, fixed using 3.7% formaldehyde (Fisher Scientific, Saint-Laurent, QC, Canada), permeabilized with Triton X-100 (0.1% (v/v) in PBS, Mallinckrodt, Thermo Fisher Scientific, Saint-Laurent, QC, Canada) and blocked by the addition of a solution of 5% (w/v) bovine serum albumin (BSA, MilliporeSigma, Oakville, ON, Canada) in PBS. Next, the cells were incubated overnight at 4 °C with the primary mouse anti-H2AX pS139 antibody (1:1000, MilliporeSigma) followed by incubation at room temperature with the secondary anti-mouse IgG Alexa Fluor 594 antibody (1:1000, Invitrogen, Burlington, ON, Canada) for 1 h. After washing with PBS, the cells were then stained with DAPI (2 μg mL^{-1}, final concentration) for 5 min in a blocking buffer containing 0.01% (v/v) Triton X-100 and 1% (v/v) BSA in PBS and washed. Finally, the coverslips were mounted on microscope slides using ProLong Glass Antifade Mountant (Invitrogen, Thermo Fisher Scientific, Saint-Laurent, QC, Canada) and air-dried at room temperature in the dark. Cell slides were examined using a Zeiss LSM 800 confocal microscope (Zeiss Canada, Toronto, ON, Canada) with images acquired using the Zeiss Zen microscopy software and processed with Fiji 2.9.0 software (NIH, MD, USA).[52]

4.2.5 DHODH inhibition. The DHODH inhibition assay was performed as described by Bouzriba et al. to evaluate the ability of PYRUB-SOs to inhibit the activity of DHODH.[26] Briefly, the assay buffer was prepared by combining the following solutions: 50 mM Tris–HCl (Fisher Scientific, Edmonton, AB, Canada), 150 mM KCl (VWR International, Mont-Royal, QC, Canada), and 0.1% Triton X-100 (pH 8). Then, the assay mix was prepared by adding 0.1 mM decyl ubiquinone (DUQ, MilliporeSigma), 1 mM dihydroorotate (DHO, MilliporeSigma), and 0.06 mM DCIP (MilliporeSigma) to the assay buffer. Then, 99.5 μL of the assay mix solution was dispensed into a preheated 96-well plate (15 min at 37 °C). Subsequently, 0.25 μL of the tested compound solutions (10, 1, 0.1, 0.01, and 0.001 μM) were added to the preheated plate in duplicate. The reaction was then initiated by adding 0.25 μL (25 ng) of DHODH (Abcam, Cambridge, MA, USA) to the plate's wells. DCIP reduction was monitored at 610 nm for 90 min at 37 °C using a SpectraMax® i3x plate reader (Molecular Devices). The inhibitory activity was determined by calculating the slope of the linear curves and comparing them to the DMSO used as excipient (0.25% (v/v)). The IC_{50} was determined using nonlinear regression by plotting the percentage of activity against the log concentrations with GraphPad Prism 10.1.2 (GraphPad Software). Each experiment was repeated three times, and the errors were expressed as SEM.

4.2.6 Differentiation of AML cells. MOLM-13 and THP-1 cells were suspended in 6-well plates at a density of 8×10^5 cells per well and were treated with PYRUB-SOs **20** or **21** for 120 h at either 2- or 10-fold their respective IC_{50}. Brequinar was used as a positive control while DMSO (0.1%) was used

as the excipient. After the treatment, the cells were collected, centrifuged, washed with PBS (1% (v/v) BSA), and normalized to 10 million cells per mL. The cells were then resuspended in a blocking buffer containing 10% human serum (MilliporeSigma) for 15 min at room temperature. After the blocking step, the cells were stained with antibodies specific to human myeloid cell surface antigens APC-CD11b (BD Biosciences) and FITC-CD14 (BioLegend, San Diego, CA, USA) for 30 min at 4 °C. Then, the cells were washed and resuspended in PBS containing Nuclear Blue (1:8000, AAT Bioquest, Pleasanton, CA, USA) acting as a cell viability marker. To investigate the dose–response effect on cell differentiation, PUB-SOs **20** and **21** were used at 0.1, 0.3, 1, 3, 7, and 10-fold their respective IC_{50} to determine the half-maximal effective concentration (EC_{50}) in THP-1. Finally, cell differentiation was determined using a Symphony A1 flow cytometer (BD Biosciences) and conducted only on viable cells. FlowJo 10.10.0 software (BD Biosciences) was used to analyze the data. Each experiment was conducted in triplicate, and errors are presented as the standard error of the mean (SEM).

4.2.7 Metabolic stability assay using liver microsomes. The metabolic stability was assessed using MLM, RLM and HLM obtained from Corning Life Science (Thermo Fisher Scientific, Montreal, QC, Canada), XenoTech (Kansas City, KS, USA) and Gibco (Thermo Fisher Scientific, Saint-Laurent, QC, Canada), respectively. First, a master mix solution was prepared in a culture tube consisting of 745 μL of ultrapure water, 200 μL of PBS 0.5 M (pH 7.4), 10 μL of NADP$^+$ solution, 10 μL of Regeneration System, and 25 μL of the corresponding thawed liver microsomes. This mixture was then incubated at 37 °C for 5 min in a shaking bath at 120 rpm. The enzymatic reaction was initiated by adding 1 μL of the selected PYRUB-SO, freshly dissolved in DMSO (400 μM), to the master mix solution (100 μL total volume). Subsequently, 100 μL aliquots for each compound underwent incubation for 0, 30 or 60 min at 37 °C. After the incubation period, 100 μL of cold MeOH was added to each aliquot to end the enzymatic reaction. The resulting mixture was centrifuged for 5 min at 15 000g, and the supernatant (20 μL) was subjected to analysis by UHPLC-UV equipped with a 2998 PDA detector (Waters). Detection was done at a wavelength of 280 nm, and the experiment was performed thrice. Finally, the $t_{1/2}$ and Cl_{int} were calculated using the following equations:

$$t_{1/2} = \ln 2 / -k$$

$$Cl_{int} = (0.693/t_{1/2}) \times (\text{volume of incubation/microsomes concentration})$$

4.3 In silico evaluation

4.3.1 Molecular docking of PYRUB-SOs in the brequinar-binding site of DHODH. Docking experiments were performed as described by Bouzriba et al.[26] using the Molecular Operating Environment (MOE) software version 2022.02 from Chemical Computing Group (Montreal, QC,

Canada). PYRUB-SOs **20** and **21** were drawn in ChemDraw software version 22.2.0 (PerkinElmer, Shelton, CT, USA) and imported into MOE as SDF files for docking studies. The X-ray crystallographic structure of the DHODH complexed with 6-fluoro-2-[2-methyl-4-phenoxy-5-(propan-2-yl)phenyl]quinoline-4-carboxylic acid (C44), an analog of brequinar was obtained from the RCSB Protein Data Bank (ID: 4IGH at 1.3 Å resolution) and loaded into the MOE software. The protein underwent preparation using the QuickPrep tool with default settings, which included adding hydrogen atoms and partial charges, adjusting Asn/Gln/His orientations, optimizing the H-bond network, removing water molecules farther than 4.5 Å from the ligand and receptor, and conducting energy minimization (RMS gradient of 0.1 kcal mol^{-1} Å^{-1}). Following the preparation of the protein, the ligand was isolated, and the binding site was defined with all amino acids within 4.5 Å of brequinar and the flavin mononucleotide (FMN). Subsequently, energy minimization of the brequinar-binding site with ligands was performed before docking DHODH inhibitors. Default settings were applied to all atoms, incorporating the absence of restriction, utilizing the Amber10 force field, ensuring system charges were reasonable, maintaining water molecule rigidity, and employing a gradient of 0.1 RMS kcal mol^{-1} Å^{-2}. The surface hydrophobicity and hydrophilicity of the DHODH binding site were mapped using the Surface and Map tool with default settings. PYRUB-SOs **20** and **21** were docked into the brequinar-binding site using selected atoms from the receptor and selected residues from the binding site. Different conformations, interactions with amino acids at the active site, and complex energies were analyzed and documented. Images of the most stable conformer in the brequinar-binding site were captured in both 2D and 3D models.

4.4 Statistical analysis

All data are presented as the means ± standard error of the mean (SEM), derived from at least three independent experiments. Statistical analyses were conducted using GraphPad Prism version 10.1.2. Group comparisons were performed using one-way analysis of variance (ANOVA), followed by Dunnett's test for multiple comparisons against the control group. Differences were considered statistically significant at $p < 0.05$.

Data availability

The data supporting this article have been included as part of the ESI.†

Author contributions

Vincent Ouellette: conceptualization, methodology, validation, formal analysis, investigation, data curation, writing – original draft preparation, writing – review and editing, supervision, project administration. Chahrazed Bouzriba: conceptualization, methodology, validation, formal analysis, investigation, data curation, writing – review and editing, supervision, project administration. Atziri Corin Chavez Alvarez: methodology, validation, formal analysis, investigation, writing, review and editing. Geneviève Hamel-Côté: methodology, validation, formal analysis, investigation, writing, review and editing. Sébastien Fortin: conceptualization, methodology, validation, formal analysis, investigation, resources, data curation, writing – original draft preparation, writing – review and editing, supervision, project administration and funding acquisition.

Conflicts of interest

The authors declare that there are no conflicts of interest.

Acknowledgements

References

1 F. Bray, M. Laversanne, H. Sung, J. Ferlay, R. L. Siegel, I. Soerjomataram and A. Jemal, Global cancer statistics 2022: GLOBOCAN estimates of incidence and mortality worldwide for 36 cancers in 185 countries, *Ca-Cancer J. Clin.*, 2024, **74**, 229–263.

2 E. Papaemmanuil, M. Gerstung, L. Bullinger, V. I. Gaidzik, P. Paschka, N. D. Roberts, N. E. Potter, M. Heuser, F. Thol and N. Bolli, Genomic classification and prognosis in acute myeloid leukemia, *N. Engl. J. Med.*, 2016, **374**, 2209–2221.

3 F. Ferrara and C. A. Schiffer, Acute myeloid leukaemia in adults, *Lancet*, 2013, **381**, 484–495.

4 National Cancer Institute (NIH), Cancer stat facts: leukemia - acute myeloid leukemia (AML), **https://seer.cancer.gov/statfacts/html/amyl.html**, (accessed May 4, 2024).

5 H. Döhner, E. Estey, D. Grimwade, S. Amadori, F. R. Appelbaum, T. Büchner, H. Dombret, B. L. Ebert, P. Fenaux, R. A. Larson, R. L. Levine, F. Lo-Coco, T. Naoe, D. Niederwieser, G. J. Ossenkoppele, M. Sanz, J. Sierra, M. S. Tallman, H.-F. Tien, A. H. Wei, B. Löwenberg and C. D. Bloomfield, Diagnosis and management of AML in adults:

2017 ELN recommendations from an international expert panel, *Blood*, 2017, **129**, 424–447.

6 H. Dombret and C. Gardin, An update of current treatments for adult acute myeloid leukemia, *Blood*, 2016, **127**, 53–61.

7 C. D. DiNardo and J. E. Cortes, Mutations in AML: prognostic and therapeutic implications, *Hematology*, 2016, **2016**, 348–355.

8 A. E. Perl, G. Martinelli, J. E. Cortes, A. Neubauer, E. Berman, S. Paolini, P. Montesinos, M. R. Baer, R. A. Larson and C. Ustun, Gilteritinib or chemotherapy for relapsed or refractory FLT3-mutated AML, *N. Engl. J. Med.*, 2019, **381**, 1728–1740.

9 D. B. Sykes, Y. S. Kfoury, F. E. Mercier, M. J. Wawer, J. M. Law, M. K. Haynes, T. A. Lewis, A. Schajnovitz, E. Jain, D. Lee, H. Meyer, K. A. Pierce, N. J. Tolliday, A. Waller, S. J. Ferrara, A. L. Eheim, D. Stoeckigt, K. L. Maxcy, J. M. Cobert, J. Bachand, B. A. Szekely, S. Mukherjee, L. A. Sklar, J. D. Kotz, C. B. Clish, R. I. Sadreyev, P. A. Clemons, A. Janzer, S. L. Schreiber and D. T. Scadden, Inhibition of dihydroorotate dehydrogenase overcomes differentiation blockade in acute myeloid leukemia, *Cell*, 2016, **167**, 171–186.

10 S. Christian, C. Merz, L. Evans, S. Gradl, H. Seidel, A. Friberg, A. Eheim, P. Lejeune, K. Brzezinka, K. Zimmermann, S. Ferrara, H. Meyer, R. Lesche, D. Stoeckigt, M. Bauser, A. Haegebarth, D. B. Sykes, D. T. Scadden, J.-A. Losman and A. Janzer, The novel dihydroorotate dehydrogenase (DHODH) inhibitor BAY 2402234 triggers differentiation and is effective in the treatment of myeloid malignancies, *Leukemia*, 2019, **33**, 2403–2415.

11 S. Sainas, A. C. Pippione, E. Lupino, M. Giorgis, P. Circosta, V. Gaidano, P. Goyal, D. Bonanni, B. Rolando, A. Cignetti, A. Ducime, M. Andersson, M. Järvå, R. Friemann, M. Piccinini, C. Ramondetti, B. Buccinnà, S. Al-Karadaghi, D. Boschi, G. Saglio and M. L. Lolli, Targeting myeloid differentiation using potent 2-hydroxypyrazolo[1,5-*a*]pyridine scaffold-based human dihydroorotate dehydrogenase inhibitors, *J. Med. Chem.*, 2018, **61**, 6034–6055.

12 T. A. Lewis, D. B. Sykes, J. M. Law, B. Muñoz, J. K. Rustiguel, M. C. Nonato, D. T. Scadden and S. L. Schreiber, Development of ML390: a human DHODH inhibitor that induces differentiation in acute myeloid leukemia, *ACS Med. Chem. Lett.*, 2016, **7**, 1112–1117.

13 M. Löffler, L. D. Fairbanks, E. Zameitat, A. M. Marinaki and H. A. Simmonds, Pyrimidine pathways in health and disease, *Trends Mol. Med.*, 2005, **11**, 430–437.

14 D. B. Sykes, The emergence of dihydroorotate dehydrogenase (DHODH) as a therapeutic target in acute myeloid leukemia, *Expert Opin. Ther. Targets*, 2018, **22**, 893–898.

15 A. K. Mohamad Fairus, B. Choudhary, S. Hosahalli, N. Kavitha and O. Shatrah, Dihydroorotate dehydrogenase (DHODH) inhibitors affect ATP depletion, endogenous ROS and mediate S-phase arrest in breast cancer cells, *Biochimie*, 2017, **135**, 154–163.

16 S. Sainas, A. Pippione, D. Boschi, V. Gaidano, P. Circosta, A. Cignetti, F. Dosio and M. Lolli, DHODH inhibitors and

17 S. Sainas, M. Giorgis, P. Circosta, G. Poli, M. Alberti, A. Passoni, V. Gaidano, A. C. Pippione, N. Vitale, D. Bonanni, B. Rolando, A. Cignetti, C. Ramondetti, A. Lanno, D. M. Ferraris, B. Canepa, B. Buccinnà, M. Piccinini, M. Rizzi, G. Saglio, S. Al-Karadaghi, D. Boschi, R. Miggiano, T. Tuccinardi and M. L. Lolli, Targeting acute myelogenous leukemia using potent human dihydroorotate dehydrogenase inhibitors based on the 2-hydroxypyrazolo[1,5-*a*]pyridine scaffold: SAR of the aryloxyaryl moiety, *J. Med. Chem.*, 2022, **65**, 12701–12724.

18 A. Branstrom, L. Cao, B. Furia, C. Trotta, M. Santaguida, J. D. Graci, J. M. Colacino, B. Ray, W. Li, J. Sheedy, A. Mollin, S. Yeh, R. Kong, R. Sheridan, J. D. Baird, K. O'Keefe, R. Spiegel, E. Goodwin, S. Keating and M. Weetall, Emvododstat, a potent dihydroorotate dehydrogenase inhibitor, is effective in preclinical models of acute myeloid leukemia, *Front. Oncol.*, 2022, **12**, 832816.

19 H. Kamli, G. S. Zaman, A. Shaikh, A. A. Mobarki and P. Rajagopalan, A combined chemical, computational, and in vitro approach identifies SBL-105 as novel DHODH inhibitor in acute myeloid leukemia cells, *Oncol. Res.*, 2022, **28**, 899–911.

20 M. Schattenkirchner, The use of leflunomide in the treatment of rheumatoid arthritis: an experimental and clinical review, *Immunopharmacology*, 2000, **47**, 291–298.

21 Z. Jianbiao, Q. Jessie Yiying, N. Yvonne, C. Jing-Yuan, T. Sabrina Hui-Min, L. Baohong, T. Tuan Zea, H. Hiroki, O. Motomi, S. Qihui, A. G. L. Ooi, L. Bertil, M. Mark and C. Wee-Joo, ASLAN003, a potent dihydroorotate dehydrogenase inhibitor for differentiation of acute myeloid leukemia, *Haematologica*, 2020, **105**, 2286–2297.

22 G. J. Peters, S. L. Sharma, E. Laurensse and H. M. Pinedo, Inhibition of pyrimidine *de novo* synthesis by DUP-785 (NSC 368390), *Invest. New Drugs*, 1987, **5**, 235–244.

23 V. Turcotte, S. Fortin, F. Vevey, Y. Coulombe, J. Lacroix, M.-F. Côté, J.-Y. Masson and R. C.-Gaudreault, Synthesis, biological evaluation, and structure-activity relationships of novel substituted *N*-phenyl ureidobenzenesulfonate derivatives blocking cell cycle progression in S-phase and inducing DNA double-strand breaks, *J. Med. Chem.*, 2012, **55**, 6194–6208.

24 M. Gagné-Boulet, H. Moussa, J. Lacroix, M.-F. Côté, J.-Y. Masson and S. Fortin, Synthesis and biological evaluation of novel *N*-phenyl ureidobenzenesulfonate derivatives as potential anticancer agents. Part 2. Modulation of the ring B, *Eur. J. Med. Chem.*, 2015, **103**, 563–573.

25 M. Gagné-Boulet, C. Bouzriba, M. Godard and S. Fortin, Preparation, characterisation and biological evaluation of new *N*-phenyl amidobenzenesulfonates and *N*-phenyl ureidobenzenesulfonates inducing DNA double-strand breaks. Part 3. Modulation of ring A, *Eur. J. Med. Chem.*, 2018, **155**, 681–694.

26 C. Bouzriba, L. Larcher, M. Gagné-Boulet and S. Fortin, *N*-phenyl ureidobenzenesulfonates, a novel class of promising

leukemia: an emergent interest for new myeloid differentiation agents, *Drugs Future*, 2018, **43**, 823–834.

human dihydroorotate dehydrogenase inhibitors, *Bioorg. Med. Chem.*, 2020, **28**, 115739.

27 C. Bouzriba, A. C. Chavez Alvarez, V. Ouellette, M. Gagné-Boulet, G. Hamel-Côté, D. Bastien, I. Laverdière and S. Fortin, *N*-Phenyl ureidobenzenesulfonates, a novel class of human dihydroorotate dehydrogenase inhibitors inducing differentiation and apoptosis in acute myeloid leukemia cells, *Biomed. Pharmacother.*, 2024, **181**, 117717.

28 A. Daina, O. Michielin and V. Zoete, SwissADME: a free web tool to evaluate pharmacokinetics, drug-likeness and medicinal chemistry friendliness of small molecules, *Sci. Rep.*, 2017, **7**, 42717.

29 A. J. Cruz-Cabeza, Acid–base crystalline complexes and the pKa rule, *CrystEngComm*, 2012, **14**, 6362–6365.

30 C. G. Wermuth and P. H. Stahl, *Handbook of pharmaceutical salts: properties, selection, and use*, Verlag Helvetica Chimica Acta, Zürich, 2nd edn, 2011.

31 W. M. Haynes, *CRC Handbook of Chemistry and Physics*, CRC Press, 97th edn, 2016.

32 S. Sowmiah, J. M. S. S. Esperança, L. P. N. Rebelo and C. A. M. Afonso, Pyridinium salts: from synthesis to reactivity and applications, *Org. Chem. Front.*, 2018, **5**, 453–493.

33 W. Li, F. Xu, W. Shuai, H. Sun, H. Yao, C. Ma, S. Xu, H. Yao, Z. Zhu, D.-H. Yang, Z.-S. Chen and J. Xu, Discovery of novel quinoline-chalcone derivatives as potent antitumor agents with microtubule polymerization inhibitory activity, *J. Med. Chem.*, 2019, **62**, 993–1013.

34 S. K. Nechipadappu and D. R. Trivedi, Structural and physicochemical characterization of pyridine derivative salts of anti-inflammatory drugs, *J. Mol. Struct.*, 2017, **1141**, 64–74.

35 N. Mahé, B. Nicolaï, H. Allouchi, M. Barrio, B. Do, R. Céolin, J.-L. Tamarit and I. B. Rietveld, Crystal structure and solid-state properties of 3,4-diaminopyridine dihydrogen phosphate and their comparison with other diaminopyridine salts, *Cryst. Growth Des.*, 2013, **13**, 708–715.

36 I. M. McLay, F. Halley, J. E. Souness, J. McKenna, V. Benning, M. Birrell, B. Burton, M. Belvisi, A. Collis, A. Constan, M. Foster, D. Hele, Z. Jayyosi, M. Kelley, C. Maslen, G. Miller, M.-C. Ouldelhkim, K. Page, S. Phipps, K. Pollock, B. Porter, A. J. Ratcliffe, E. J. Redford, S. Webber, B. Slater, V. Thybaud and N. Wilsher, The discovery of RPR 200765A, a p38 MAP kinase inhibitor displaying a good oral anti-arthritic efficacy, *Bioorg. Med. Chem.*, 2001, **9**, 537–554.

37 R. J. Bastin, M. J. Bowker and B. J. Slater, Salt selection and optimisation procedures for pharmaceutical new chemical entities, *Org. Process Res. Dev.*, 2000, **4**, 427–435.

38 A. T. M. Serajuddin, Salt formation to improve drug solubility, *Adv. Drug Delivery Rev.*, 2007, **59**, 603–616.

39 National Cancer Institute (NCI), Developmental therapeutics program (DTP), NCI-60 screening methodology, **https://dtp.cancer.gov/discovery_development/nci-60/default.htm**, (accessed 25 January, 2023).

40 American Type Culture Collection (ATCC), MTT Cell Proliferation Assay, **https://www.atcc.org/products/30-1010k**, (accessed January 25, 2023).

41 Cyprotex, Microsomal stability assay, **https://www.cyprotex.com/admepk/in-vitro-metabolism/microsomal-stability**, (accessed 25 January, 2024).

42 Swiss Institute of Bioinformatics, SwissADME: General, scientific, and technical questions, **http://www.swissadme.ch/faq.php#Is_it_preferable_to_input_the_neutral_form_of_the_molecule**, (accessed 13 April, 2023).

43 P. Ertl, B. Rohde and P. Selzer, Fast calculation of molecular polar surface area as a sum of fragment-based contributions and its application to the prediction of drug transport properties, *J. Med. Chem.*, 2000, **43**, 3714–3717.

44 C. A. S. Bergström and M. Yazdanian, Lipophilicity in drug development: too much or not enough?, *AAPS J.*, 2016, **18**, 1095–1100.

45 H. Zhang, H. Xu, C. R. Ashby Jr, Y. G. Assaraf, Z.-S. Chen and H.-M. Liu, Chemical molecular-based approach to overcome multidrug resistance in cancer by targeting P-glycoprotein (P-gp), *Med. Res. Rev.*, 2021, **41**, 525–555.

46 D. Waghray and Q. Zhang, Inhibit or evade multidrug resistance P-glycoprotein in cancer treatment, *J. Med. Chem.*, 2018, **61**, 5108–5121.

47 S. Fortin, L. Wei, E. Moreau, J. Lacroix, M.-F. Côté, É. Petitclerc, L. P. Kotra and R. C.-Gaudreault, Design, synthesis, biological evaluation, and structure-activity relationships of substituted phenyl 4-(2-oxoimidazolidin-1-yl) benzenesulfonates as new tubulin inhibitors mimicking combretastatin A-4, *J. Med. Chem.*, 2011, **54**, 4559–4580.

48 S. Fortin, L. Wei, E. Moreau, J. Lacroix, M.-F. Côté, É. Petitclerc, L. P. Kotra and R. C.-Gaudreault, Substituted phenyl 4-(2-oxoimidazolidin-1-yl)benzenesulfonamides as antimitotics. Antiproliferative, antiangiogenic and antitumoral activity, and quantitative structure-activity relationships, *Eur. J. Med. Chem.*, 2011, **46**, 5327–5342.

49 Millipore, Determination of aqueous compound solubility using a 96-well filter plate to remove precipitated solids prior to UV/Vis spectroscopic analysis, **https://www.sigmaaldrich.com/deepweb/assets/sigmaaldrich/product/documents/103/938/an1730en00.pdf**, (accessed 25 March, 2023).

50 B. Hoelke, S. Gieringer, M. Arlt and C. Saal, Comparison of nephelometric, UV-spectroscopic, and HPLC methods for high-throughput determination of aqueous drug solubility in microtiter plates, *Anal. Chem.*, 2009, **81**, 3165–3172.

51 T. Sou and C. A. S. Bergström, Automated assays for thermodynamic (equilibrium) solubility determination, *Drug Discovery Today: Technol.*, 2018, **27**, 11–19.

52 J. Schindelin, I. Arganda-Carreras, E. Frise, V. Kaynig, M. Longair, T. Pietzsch, S. Preibisch, C. Rueden, S. Saalfeld, B. Schmid, J.-Y. Tinevez, D. J. White, V. Hartenstein, K. Eliceiri, P. Tomancak and A. Cardona, Fiji: an open-source platform for biological-image analysis, *Nat. Methods*, 2012, **9**, 676–682.